

# **Technical Note: Water Vapor climatologies in the extra-tropical Upper Troposphere and Lower Stratosphere derived from a Synthesis of Passenger and Research Aircraft Measurements**

Patrick Konjari<sup>1,4</sup>, Christian Rolf<sup>1</sup>, Michaela I. Hegglin<sup>1,5,6</sup>, Susanne Rohs<sup>2</sup>, Yun Li<sup>2</sup>, Andreas Zahn<sup>3</sup>, Harald Bönisch<sup>3</sup>, [Philippe Nedelec](#)<sup>7</sup>, Martina Krämer<sup>1,4</sup>, and Andreas Petzold<sup>2,5</sup>

<sup>1</sup>Forschungszentrum Jülich GmbH, Institute of Climate and Energy Systems 4 – Stratosphere, Jülich, Germany

<sup>2</sup>Forschungszentrum Jülich GmbH, Institute of Climate and Energy Systems 3 – Troposphere, Jülich, Germany

<sup>3</sup>Karlsruhe Institute of Technology, Institute of Meteorology and Climate Research, Karlsruhe, Germany

<sup>4</sup>Johannes Gutenberg-Universität Mainz, IPA, Mainz, Germany

<sup>5</sup>Bergische Universität Wuppertal, Institute for Atmospheric and Environmental Research, Wuppertal, Germany

<sup>6</sup>University of Reading, Department of Meteorology, Reading, UK

<sup>7</sup>Laboratoire d'Aérodynamique, Université de Toulouse, CNRS, UPS, Toulouse, France

**Correspondence:** Patrick Konjari (p.konjari@fz-juelich.de)

## **Abstract.**

~~Water vapor (H<sub>2</sub>O) is a key trace gas in the upper troposphere (UT) and lowermost stratosphere (LMS), as it significantly influences the Earth's climate system through its roles in radiative forcing and cloud formation. However, accurate knowledge of the amount of H<sub>2</sub>O in this atmospheric region is still insufficient due to the difficulty and lack of precise in-situ and space-borne measurements.~~ This study presents a new methodology to derive adjusted H<sub>2</sub>O climatologies for the extra-tropical UT/LMS from regular measurements aboard passenger aircraft between 1994 and 2022 within the IAGOS (In-service Aircraft for a Global Observing System) research infrastructure. ~~To this end, a~~ A synthesis of mean H<sub>2</sub>O is performed by sampling air mass bins of similar origin and thermodynamic conditions relative to the tropopause between a dataset from 60.000 flights ~~applying~~ employing the IAGOS-MOZAIC and -CORE ~~compact~~ capacitive hygrometer (ICH) and a ~~data set~~ dataset of 10 500 flights using the more sophisticated IAGOS-CARIBIC hygrometer. The analysis is, in combination with ECMWF ERA5 meteorological data, accomplished for the extra-tropical northern hemisphere, where the datasets have the largest common coverage. We find very good agreement in the UT, but a systematic positive humidity bias in the ICH measurements for the LMS. To account for this bias, mean H<sub>2</sub>O of the ICH are adjusted to the IAGOS-CARIBIC measurements based on a new mapping and adjustment approach. After applying this new method, the LMS H<sub>2</sub>O measurements are in good agreement 15 between all investigated platforms. The extensive H<sub>2</sub>O data set from the compact IAGOS sensor can now be used to produce highly resolved H<sub>2</sub>O climatologies for the climatically sensitive LMS region.

## 1 Introduction

Over the past decades, upper tropospheric and lowermost stratospheric (UT/LMS) water vapor ( $H_2O$ ) has gained increasing attention due to its significant impact on the global climate system (IPCC, 2023). Apart from the influence on ozone concentration (Kirk-Davidoff et al., 1999) and cirrus cloud formation, even small variations in UT/LMS  $H_2O$  lead to substantial changes in radiative forcing (Riese et al., 2012; Banerjee et al., 2019; Gettelman et al., 2011). Radiative forcing calculations suggest that the increase in stratospheric  $H_2O$  of 0.8 ppmv as derived from balloon soundings between 1980-2000 could have accounted for 30 % of the total anthropogenic forcing during that time period (Forster and Shine, 2002). On the other hand, satellite-borne measurements spanning back to the 1980s, have not shown significant long-term trends in stratospheric  $H_2O$  over several decades (Hegglin et al., 2014; Konopka et al., 2022). For the future, however, most global climate models predict an increase in stratospheric  $H_2O$  (e.g., Banerjee et al., 2019; Huang et al., 2020) and a corresponding surface warming-total stratospheric water vapor radiative feedback parameter of 0.2 – 0.3 W/mm<sup>2</sup> per 1 Kelvin of global-surface warming (Forster and Shine, 2002; Huang et al., 2020; Nowack et al., 2023). Nevertheless, there are still significant uncertainties in predicting the radiative forcing resulting from changes in stratospheric  $H_2O$  (Huang et al., 2020). One of the reasons is that the low stratospheric  $H_2O$  concentrations below 10 ppmv, and the even smaller changes are difficult to detect with required statistical significance. Therefore, accurate detection of UT/LMS  $H_2O$ , as well as trends on-a-at high temporal and spatial resolution are essential to better understand the role of  $H_2O$  in this part of the atmosphere for the global climate system.

Global observation of  $H_2O$  in the UT/LMS is provided by space-borne remote sensing instruments, such as the Microwave Limb Sounder (Hegglin et al., 2013). Due to their limited vertical resolution of several kilometers, however, the space-borne observations cannot adequately resolve the high vertical gradients of  $H_2O$  across the extra-tropical tropopause layer (Gettelman et al., 2011; Zahn et al., 2014). To address this limitation and provide UT/LMS  $H_2O$  profiles with a high vertical resolution, airborne in-situ measurements play a crucial role. The IAGOS (In-service Aircraft for a Global Observing System; www.iagos.org) database offers  $H_2O$  measurements from over 60.000 passenger aircraft flights, enabling to-resolve-the-the resolution of the strong vertical and temporal  $H_2O$  variations in the UT/LMS of the extra-tropical northern hemisphere (Zahn et al., 2014; Petzold et al., 2020). For instance, based on IAGOS observations over North America, the North Atlantic, and Europe (40°-60°N each), Petzold et al. (2020) were able to resolve the pronounced seasonality of UT/LMS  $H_2O$  in these regions with a vertical resolution of 0.3 km. This study revealed a near doubling of the  $H_2O$  mixing ratio during summer compared to winter in the UT and the first kilometer above the thermal tropopause, with the strongest seasonality observed over the North Atlantic. The investigation of these seasonal and spatial UT/LMS  $H_2O$  variations based on IAGOS measurements helps to quantify and understand the processes that control the temporal and spatial variability of  $H_2O$ . These can be seasonal variations attributed to the Brewer-Dobson circulation and isentropic transport or short-term micro- to mesoscale  $H_2O$  mixing between troposphere and stratosphere associated with turbulence and diabatic processes like overshooting convection (Gettelman et al., 2011). A better understanding of these processes helps to improve their representation in climate models. In this context, a-large amount-of- $H_2O$ -the large quantity in-situ measurements-as- $H_2O$  measurements provided by IAGOS is of-crucial-importance to-improve-important-to-improving the accuracy of future  $H_2O$  and corresponding radiative forcing trends based on climate

model predictions.

The IAGOS database consists of three datasets with instrument packages of different ~~sorts~~kinds: IAGOS-MOZAIC (MOZAIC: Measurement of Ozone by AIRBUS In-Service Aircraft; Marenco et al., 1998), IAGOS-CORE ((Petzold et al., 2015)) and IAGOS-CARIBIC (~~Dyroff et al., 2015~~)(Civil Aircraft for the Regular Investigation of the Atmosphere Based on an Instrument Container; Dyroff et al. (2015)). The MOZAIC project was the predecessor program to IAGOS-CORE, and the data were integrated into the IAGOS database afterwards. Combined, IAGOS-MOZAIC and -CORE contain ~60.000 flights, both providing humidity measurements by a compact ~~humidity-capacity-capacitive humidity~~ sensor of same type (ICH; Neis et al. (2015a)). Compared to IAGOS-MOZAIC and -CORE, the IAGOS-CARIBIC dataset consists of a relatively small number of flights of ~500. The IAGOS-CARIBIC package consists of sophisticated instruments, enabling high precision measurements of H<sub>2</sub>O even for very low stratospheric concentrations (Zahn et al., 2014). The ICH measurements, however, were found to ~~loose-lose~~ precision for very dry stratospheric air masses (~~Rolf et al., 2023~~)(Kunz et al., 2008; Rolf et al., 2023). In a previous intercomparison of IAGOS H<sub>2</sub>O observations (at that time taken in the framework of the MOZAIC project), and research-aircraft based observations as part of the SPURT (Spurenstofftransport in der Tropopausenregion, trace gas transport in the tropopause region; Engel et al. (2006)) project, a lower H<sub>2</sub>O threshold for precise measurements of 10 ppmv was determined for the ICH at conditions typical of the extra-tropical LMS (Kunz et al., 2008). This lower detection limit for the ICH ~~instruments was further constraint to~~ instrument was later determined to be 30 ppmv by means of a dedicated hygrometer intercomparison study (Rolf et al., 2023).

The aim of this study is to provide an improved dataset by mapping and adjusting the IAGOS-MOZAIC and -CORE measurements to observations from more precise instruments. Therefore, in order to quantify the H<sub>2</sub>O bias of IAGOS-MOZAIC and -CORE in the LMS, the first step of this study is to compare these data with the IAGOS-CARIBIC measurements that are able to resolve low LMS H<sub>2</sub>O. Furthermore, sophisticated campaign measurements from 500 flights summarized in the JULIA (JüLich In-situ Airborne Data Base; Krämer et al., 2020) data base are included in the comparison.

The main challenge ~~of this study~~ is to devise an approach that allows for a valid intercomparison of the in-situ H<sub>2</sub>O datasets, despite the limited amount of IAGOS-CARIBIC and JULIA data, and the fact that the measurements of the datasets were performed on different platform at different times and in different regions. To address this challenge, we apply a robust new mapping methodology that enables an accurate comparison of H<sub>2</sub>O in air masses of similar atmospheric origin, thermodynamic conditions and seasons. Through this comparison, we can identify and quantify biases in the H<sub>2</sub>O measurements by IAGOS-MOZAIC and -CORE in the LMS.

Based on the results of ~~the this~~ intercomparison, we develop an adjustment methodology to the IAGOS-MOZAIC and -CORE H<sub>2</sub>O datasets in the LMS. This methodology allows ~~us~~ to account for the biases identified in the intercomparison, ensuring improved accuracy in the representation of the H<sub>2</sub>O variability in the ~~northern mid-latitudinal~~ UT/LMS region at northern mid-latitudes.

The paper is structured as follows: In Section 2, we provide a comprehensive overview of the datasets that are utilized in the comparison presented in Section 3. Section 4 outlines the methodology employed for mapping and adjusting the IAGOS-

85 MOZAIC and -CORE LMS H<sub>2</sub>O climatologies in dry LMS regions. In Section 5, we summarize the key findings ~~of this study~~ and provide an outlook on potential future research based on the adjusted IAGOS-MOZAIC and -CORE H<sub>2</sub>O climatologies.

## 2 H<sub>2</sub>O datasets

### 2.1 Airborne in-situ H<sub>2</sub>O measurements

Two sets of IAGOS H<sub>2</sub>O data from about three decades of airborne in-situ measurements with a compact capacitive hygrometer (IAGOS capacitive hygrometer: ICH; see Section 2.1.1), IAGOS-MOZAIC and IAGOS-CORE, are the basis of this study and are combined into one dataset (IAGOS-MOZAIC&CORE). This extensive data set is validated against two others, IAGOS-CARIBIC and JULIA, which are smaller, but have measured H<sub>2</sub>O with more accurate instruments. The IAGOS-CARIBIC water instrument applies two different sensor systems (WaSul and frost point hygrometer; see Section 2.1.2). The JULIA data base primarily contains data from the high precision hygrometer FISH (Section 2.1.3). The datasets are summarized in Table 1.

95 A detailed intercomparison study of ICH, WaSul and FISH aboard a Learjet research aircraft was conducted as part of the DENCHAR project ~~and is described by~~ Rolf et al. (2023).

#### 2.1.1 H<sub>2</sub>O from passenger aircraft: IAGOS - MOZAIC & CORE

The IAGOS-MOZAIC&CORE dataset (from now on just MOZAIC&CORE) (<https://www.iagos.org/>) provides measurements of the relative humidity w.r.t. liquid ( $RH_{liq}$ ), taken by the compact capacitive sensor ICH aboard commercial aircraft in the period from 1995 to this day, and ~~derive~~-derived H<sub>2</sub>O mixing ratios. The ICH relies on a water adsorbing dielectric ~~film~~ membrane between two parallel electrodes with its dielectric capacity depending on the relative humidity of the surrounding air. Measurements are provided every 4 seconds, which corresponds to a horizontal resolution of about 1 km. The instruments are removed from the aircraft every 3 months and are calibrated against a reference frost point hygrometer in an atmospheric simulation chamber before being re-installed again. Details of the current instrument handling and data processing are described

105 by (Petzold et al., 2020).

The largest amount of the 60.000 flights in the dataset took place in the northern mid-latitudes between Europe and North America (Figure 1a). Here, at flight altitudes of 9 - 13 km, heights of up to 5 km above the tropopause can be reached, especially during the winter season on northern routes, while in the tropics only the upper troposphere is covered (Figure 1d).

#### 2.1.2 H<sub>2</sub>O from passenger aircraft: IAGOS-CARIBIC

110 The IAGOS-CARIBIC dataset (from now on just CARIBIC) provides measurements from more than 500 long-distance passenger aircraft flights (Figure 1b and e) in the period from 1997 to 2020. The instruments installed in the CARIBIC ~~packages~~ Flying Laboratory measure about 100 tracers and aerosol parameters (<https://www.CARIBIC-atmospheric.com>), including water vapor and total (gaseous, liquid and ice phase) water.

Compared to MOZAIC&CORE, measurements are taken by more advanced instrumentation. The CARIBIC water instrument

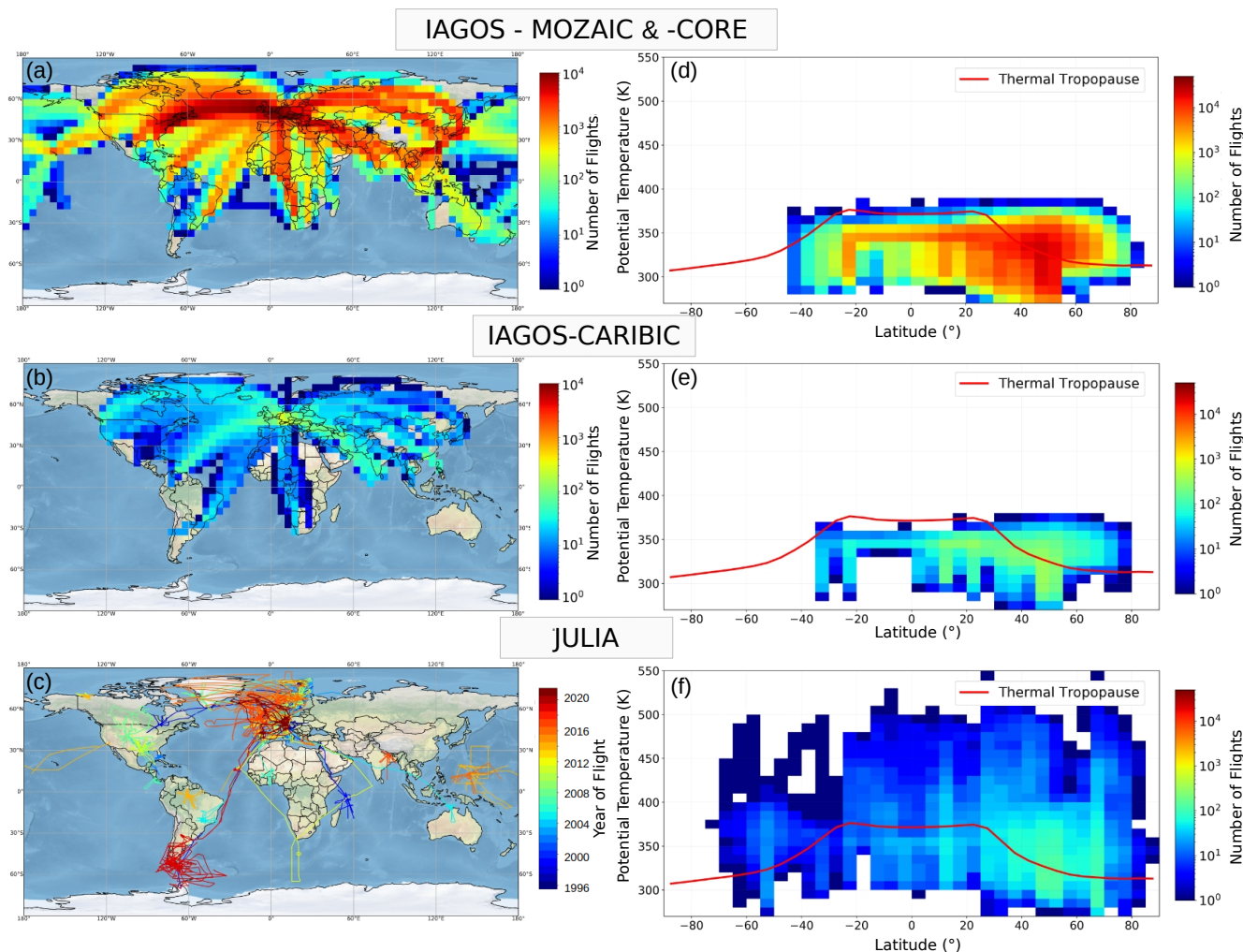


**Figure 1. Geographical distribution of H<sub>2</sub>O measurements.** The plots indicate the flight density of IAGOS-MOZAIC&CORE, IAGOS-CARIBIC, and JULIA, both horizontally (a-c) and vertically (d-f). In (a-c), the flight density is given on a 5x5° grid for the IAGOS data sets, while for JULIA the single flight tracks and corresponding years are shown. Potential temperature is taken as vertical coordinate (d-f) with a resolution of 5K and a latitude resolution of 5°; the solid red lines represent the average thermal tropopause, calculated from ERA5 data.

115 applies two different sensor systems (measurement techniques), a modified (dual-channel [PA-laser-photo-acoustic laser](#) spectrometer) WaSul sensor (for total and gasphase water) and a modified CR2 Buck frost-point hygrometer (FPH) sensor, with the FPH being used for a regular in-flight calibration of the WaSul sensor. (Dyroff et al., 2015)

**Table 1.** Summary of the UT/LS airborne in-situ H<sub>2</sub>O data sets

| Product               | Instruments  | Measurement<br>Quantity              | Time period | Accuracy                                     | Reference                                       |
|-----------------------|--|--------------------------------------|-------------|--|---|
| IAGOS-<br>MOZAIC&CORE | Capacitive Hygrometer<br>(ICH)   | RH <sub>liq</sub>                    | 1995 - 2021 | 4–7 % RH <sub>liq</sub>                      | Helten et al. (1998),<br>Neis et al. (2015a, b) |
| IAGOS-<br>CARIBIC     | Photoacoustic laser<br>spectrometer (WASUL),<br>Frost-point hygrometer | H <sub>2</sub> O<br>T <sub>dew</sub> | 1997 - 2020 | 4 % / 0.3 ppmv for<br>H <sub>2</sub> O=5ppmv | Dyroff et al. (2015)                            |
| JULIA                 | Lyman- $\alpha$ fluorescence<br>hygrometer (FISH)                      | H <sub>2</sub> O                     | 1994-2021   | 7 % $\pm$ 0.3 ppmv                           | Zöger et al. (1999);<br>Meyer et al. (2015)     |

### 2.1.3 H<sub>2</sub>O from research aircraft: JULIA

The JUElich In-situ Airborne Data Base (JULIA) contains H<sub>2</sub>O data from more than 500 research aircraft flights during 46  
120 campaigns that took place from 1994 onward. It contains precise measurements from advanced instrumentation of trace gases  
like H<sub>2</sub>O, and cloud microphysical properties (Krämer et al., 2020). H<sub>2</sub>O data are provided by instruments that have a high  
sensitivity to low stratospheric H<sub>2</sub>O, with most measurements being performed by the Fast In-situ Stratospheric Hygrometer  
(FISH; Zöger et al., 1999), which is sensitive to low UT/LMS H<sub>2</sub>O, with an accuracy of 6 - 8 % between 1 and 1000 ppmv  
(Meyer et al., 2015). In contrast to the IAGOS flights, the research aircraft flights often reach deeper into the stratosphere and  
125 also cover the tropical LS, with altitudes of up to 20 km, which corresponds to potential temperatures of more than 500 K  
(Figure 1).

## 2.2 ECMWF ERA5 reanalysis data

The ERA5 reanalysis data (Hersbach et al., 2020) from the European Centre for Medium-Range Weather Forecasts (ECMWF)  
provide meteorological parameters every hour in the period from 1959 onward. The ERA5 data are given on a 30 km horizontal  
130 resolution with 137 vertical model levels, reaching heights of up to 0.1 hPa. For this study, ERA5 data ~~is used on a~~ are used at  
reduced resolution of 6 hours and 1 x 1°, but with the original vertical resolution. Along the flight paths of passenger (IAGOS)  
and research (JULIA) aircraft, the position relative to the first and, if present, second WMO thermal tropopause as well as the  
equivalent latitude derived from the potential vorticity fields are interpolated.

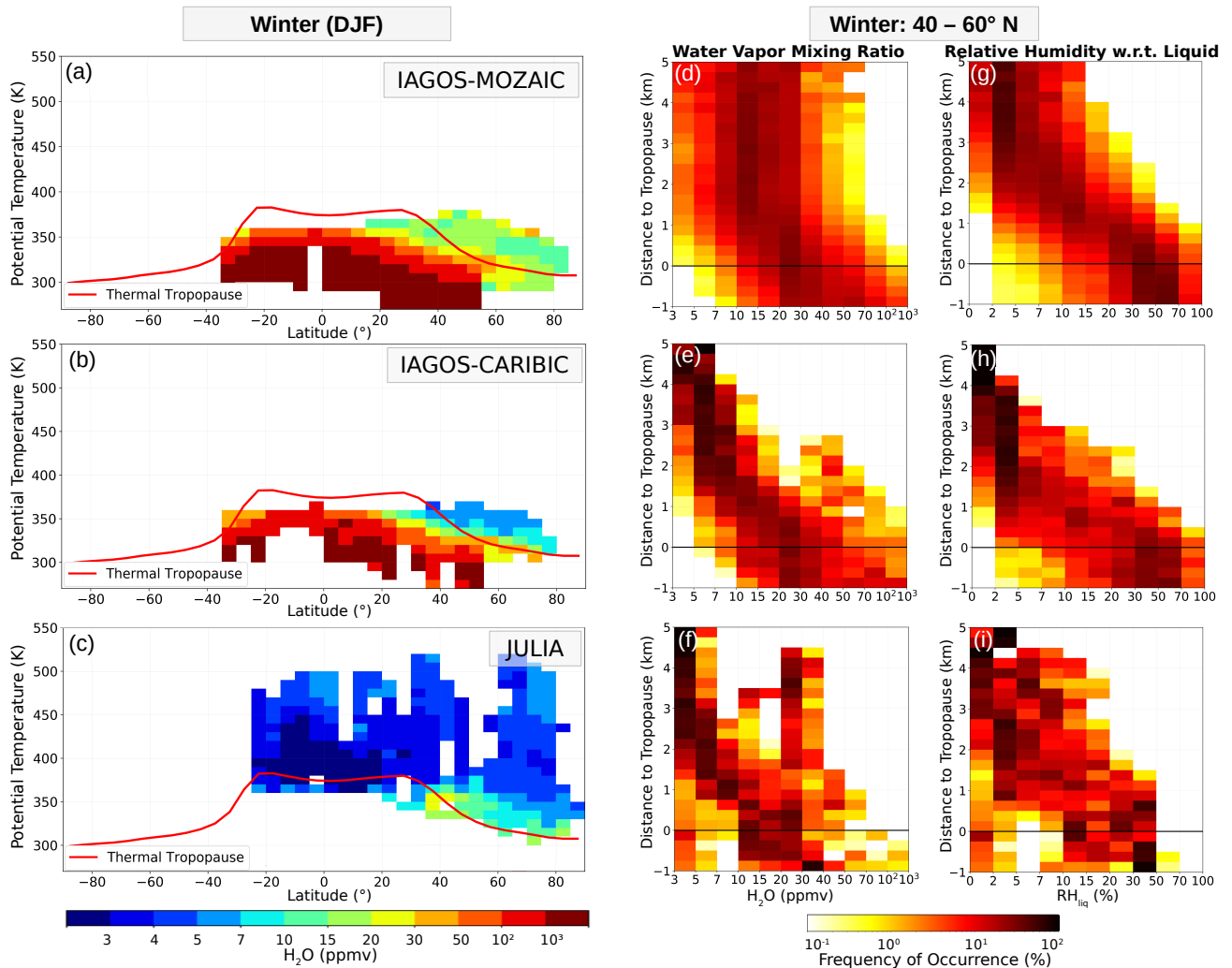


**Figure 2. Multi-annual latitudinal cross sections of  $H_2O$  for the datasets IAGOS-MOZAIC&CORE, IAGOS-CARIBIC and JULIA.** (a-c) show the winter (December-February) mean  $H_2O$  binned in  $5^\circ$  latitude  $\times$  5 K potential temperature; the solid red lines represent the average thermal tropopause, calculated from ERA5 data. For the winter season at 40 - 60°N, the probability density **relative**-in coordinates relative to the thermal tropopause ( $\Delta z$ ) and normalized per  $\Delta z$  is shown for  $H_2O$  (d-f) and  $RH_{liq}$  (g-i) .

### 3 Intercomparison of airborne in-situ $H_2O$ datasets

135 In this section, a comparative analysis of the in-situ  $H_2O$  products is performed, focusing on the UT/LMS region. Given the similar performance found in this study for the MOZAIC and CORE measurements, as detailed in Section 3.3, the primary emphasis is on the MOZAIC data, with the findings also accounting for CORE.

Figure 2a-c presents latitudinal cross-sections of  $H_2O$  for the winter (December-February) season, using a resolution of  $5^\circ$  latitude  $\times$  5 K potential temperature based on all available data from the different datasets. In the mid to high latitudes, potential

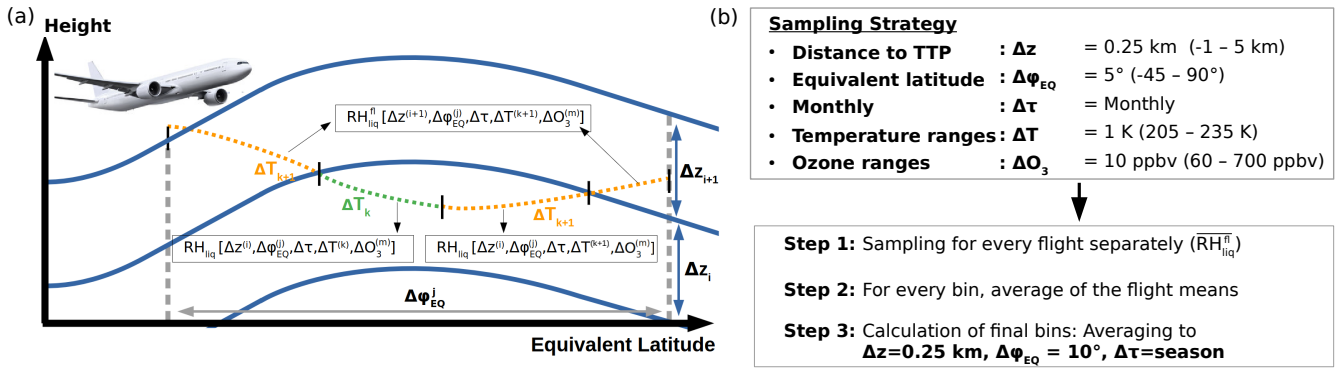


**Figure 3. Schematic illustration of the data sampling strategy to compare the different H<sub>2</sub>O products.** (a) The blue lines indicate constant height levels relative to the tropopause, and the two dashed grey lines mark a  $5^\circ$  equivalent latitude bin; ~~see~~. [The dotted line illustrates the flight path, with the different colors indicating different temperature ranges](#)<sup>3</sup>. See top box of (b) for the definition of the sampling bins of distance to the thermal tropopause ( $\Delta z$ ), equivalent latitude ( $\Delta\varphi_{EQ}$ ), time ( $\Delta\tau$ ), temperature ( $\Delta T$ ), and ozone ( $\Delta O_3$ ). The bottom box of (b) lists the different steps to derive the final sampling bins used for the intercomparison of the H<sub>2</sub>O datasets.

140 temperature levels above 350 K predominantly correspond to air masses in the LMS during the winter season. Here, the mean H<sub>2</sub>O values of MOZAIC are significantly higher (10-20 ppmv) than the values reported by CARIBIC and JULIA (5-10 ppmv). The H<sub>2</sub>O frequency distribution relative to the thermal tropopause (TTP, altitude bin width: 0.25 km) shown in Figure 2d-f for the winter 40 - 60°N domain underpins the noticeable contrasts between the three datasets. Specifically, ~~for~~ for MOZAIC, a consistent moist bias is evident from heights of 1 km above the TTP. This bias is becoming more pronounced at higher altitudes. Additionally, MOZAIC shows a more pronounced H<sub>2</sub>O variability compared to CARIBIC and JULIA at heights of 1 km above the TTP. This behavior is closely linked to the [measurement quantity magnitude of  \$RH\_{liq}\$  of the compact IAGOS humidity sensor ICH \(see Section 3.3\) measured by the ICH sensor](#). The  $RH_{liq}$  data from CARIBIC and JULIA indicate that  $RH_{liq}$  values frequently drop below 10 % at these altitudes, and they are often below 5 % at altitudes of 3 km and higher than the TTP (Figure 2h-i&i). In contrast, the  $RH_{liq}$  profile of MOZAIC displays a less strong decrease of  $RH_{liq}$  in the LMS and generally higher values compared to CARIBIC and JULIA.

150

~~As already mentioned in the Introduction, previous research campaign flights where the compact ICH sensor was operated along with the sophisticated H<sub>2</sub>O instrument FISH revealed that the sensitivity of the ICH sensor decreases significantly for very low  $RH_{liq}$  values below 10 % (Neis et al., 2015a, b).~~ The reason for this loss of sensitivity of the ICH sensor in the LMS is attributed to the adiabatic compression effect. As the air flows into the inlet towards the sensor, it undergoes heating in the range of 20 to 30 K. Consequently, even though the stratospheric humidity values are already very low, the measured values at the sensor decrease by ~~the a~~ a factor of 10, resulting in a sensitivity loss of the ICH for these very ~~small-low~~ [small-low](#) relative humidity values [below  \$\approx 10\%\$   \$RH\_{liq}\$  \(Neis et al., 2015a, b\)](#). More details about this effect are discussed in (Petzold et al., 2020). [Despite the systematic biases at low  \$RH\_{liq}\$ , the ICH sensor demonstrates a measurable response beyond the noise level, even at  \$RH\_{liq}\$  values as low as approximately 1 % \(Neis et al., 2015a; Rolf et al., 2023\).](#)

155

160 When comparing the H<sub>2</sub>O distributions shown in Figure 2e-f-e&f between JULIA and CARIBIC, both originating from sensors sensitive to low stratospheric H<sub>2</sub>O values, still some differences are ~~nevertheless~~ noticeable. First, the spatial and seasonal coverage of JULIA and CARIBIC datasets differs, contrary to the very good temporal and spatial agreement between CARIBIC and MOZAIC&CORE (Figure 1). Moreover, the research campaign measurements in JULIA were often conducted under specific atmospheric conditions, such as during ~~studies-of-troposphere-to-stratosphere exchange processes~~ events. As a result, 165 cases of anomalous H<sub>2</sub>O concentrations may be over-represented in the JULIA data set. This is evident, for instance, in a frequency of occurrence of H<sub>2</sub>O between 20 and 50 ppmv at distances of 3 km and more above the thermal tropopause (TTP) in Figure 2b-f, where the mean winter extratropical H<sub>2</sub>O values are expected to be below 10 ppmv on average (Zahn et al., 2014). However, at higher altitudes, corresponding to potential temperatures above 400 K, JULIA provides a climatological perspective of H<sub>2</sub>O from the tropics to the northern sub-polar regions (Figure 2a-c). In these potential temperature ranges, H<sub>2</sub>O 170 concentrations exhibit seasonal variations due to the Brewer-Dobson circulation, while the effects of short-term UT-to-LMS mixing processes do not significantly contribute to the H<sub>2</sub>O distribution on a short time scale in the order of days (Gettelman et al., 2011).

As discussed in this section, MOZAIC&CORE overestimate ~~low~~-H<sub>2</sub>O in most parts of the extratropical LMS due to sensor limitations in capturing low values of RH<sub>liq</sub> values that are common in this part of the atmosphere. To further quantify the 175 MOZAIC&CORE bias in the LMS, we developed an air mass mapping approach that allows for a better intercomparison with the CARIBIC H<sub>2</sub>O data. This method will be detailed in the next section.

### 3.1 Mapping approach to compare in-situ H<sub>2</sub>O datasets

A mapping approach is used as the method of evaluation of MOZAIC&CORE on the basis of CARIBIC, focusing on the primary variable measured by MOZAIC&CORE ~~measurement quantity~~, RH<sub>liq</sub>. The main challenge in this intercomparison 180 is to ensure data comparability, given the relatively small number of CARIBIC (~500 flights) compared to the large amount of MOZAIC&CORE data (together 60,000 flights). The relatively small number of CARIBIC data points could introduce non-negligible uncertainties in the statistical comparison due to the natural variability of UT/LMS H<sub>2</sub>O caused by competing transport, chemical, and mixing processes near the tropopause. ~~They affect particularly~~ These factors particularly affect the UT and the extratropical transition layer (exTL) (Zahn et al., 2014), whereas H<sub>2</sub>O above the exTL exhibits much smaller 185 variations (Gettelman et al., 2011). To minimize this uncertainty, a careful temporal and spatial sampling is performed using a geophysically-based coordinate system known to reduce sampling biases (Millan et al., 2023). The methodology is summarized in Figure 3.

Spatially, the H<sub>2</sub>O data are sampled relative to the TTP ( $\Delta z_{TTP}$ ) obtained from ERA5. The sampling starts 1 km below the TTP, with a vertical resolution of 0.25 km, and is done in equivalent latitude ranges ( $\Delta\varphi_{EQ}$ ) of 5°. Cases with double tropopauses 190 were excluded from the analysis. We found that incorporating the dynamical tropopause, defined as 2 potential vorticity units (PVU; 1 PVU = 10<sup>-6</sup> K · m<sup>2</sup> · s<sup>-1</sup> · kg<sup>-1</sup>), neither improved nor worsened the quality of the resulting intercomparison. Instead of using latitudinal mean values of H<sub>2</sub>O, means corresponding to ERA5 equivalent latitude are calculated, because the potential vorticity based equivalent latitude characterizes the latitudinal air mass origin in the UTLS (Gettelman et al., 2011), ~~which is~~

~~correlated with and the~~ corresponding H<sub>2</sub>O ~~amounts-mixing ratios~~, to some extent.

195 On a temporal scale, we calculate monthly means ( $\Delta\tau_{\text{month}}$ ) to account for the seasonal variability of UT/LMS H<sub>2</sub>O (Zahn et al., 2014; Petzold et al., 2020). Since H<sub>2</sub>O data of MOZAIC&CORE are derived from RH<sub>liq</sub> measurements, which depend on temperature, we further divide each bin ( $\Delta z_{\text{TP}}$ ,  $\Delta\varphi_{EQ}$ ,  $\Delta\tau_{\text{month}}$ ) into temperature ranges ( $\Delta T$ ) of 1 K. This temperature sampling ensures that any potential discrepancies in the sampled RH<sub>liq</sub> due to differences in the temperature distribution between MOZAIC&CORE and CARIBIC are accounted for. Additionally, the temperature at a certain height level can correlate  
200 with atmospheric conditions, which in turn can influence the H<sub>2</sub>O values. Although we also performed a potential temperature sampling, it did not yield significant differences in the final intercomparisons and was therefore not used in the final sampling strategy. The temperature sub-sampling at specific heights essentially achieves the same effect as the potential temperature sampling, given the relatively stable flight pressure levels.

To enhance the statistical comparability, we incorporate ozone measurements that were conducted during the majority of  
205 MOZAIC&CORE, and CARIBIC flights. Bethan et al. (1996) and Sprung and Zahn (2010) demonstrated that ozone measurements are effective in delineating the structure of the LMS. Above the tropopause, the characteristic increase of ozone concentrations makes it suitable as stratospheric tracer and can be indicative for stratospheric air masses to resolve UT-LMS mixing processes. Therefore, for each bin sampled above the thermal tropopause, we further sub-sample the air masses based on ozone concentrations in steps of  $\Delta O_3 = 10$  ppbv, spanning the range from 60 to 700 ppbv.

210 The binning process ( $\Delta z_{\text{TP}}$ ,  $\Delta\varphi_{EQ}$ ,  $\Delta\tau_{\text{month}}$ ,  $\Delta T$ ,  $\Delta O_3$ ) is conducted for each flight individually (Figure 3a; Figure 3b - Step 1). For every measurement that falls into a respective sampling bin and flight, we compute the sampling means  $\overline{\text{RH}}_{\text{liq}}^{\text{fl}}$  (see Figure 3a). To derive a relevant sampling mean, a minimum of 10 data points is required per bin and flight. Subsequently, for each of these bins, the arithmetic mean is computed from all the mean values obtained from the individual flights:

$$\overline{\text{RH}}_{\text{liq}}^* = \frac{1}{N_{\text{fl}}^*} \sum_{i=0}^{N_{\text{fl}}} \overline{\text{RH}}_{\text{liq}}^{\text{fl}}[i], \quad (1)$$

215 where  $N_{\text{fl}}^*$  is the total number of flights for a certain sampling bin.

Data from different flights are weighted equally to mitigate the potential influence of measurements from individual flights that might have a larger number of observations compared to most other flights. This equal weighting is particularly crucial for the sampling of CARIBIC data, where some bins may contain data from 10 flights or less, making it necessary to ensure ~~fair~~  
appropriate representation of all flights in the analysis.

220 In the final step, to ensure a sufficient number of bins with enough data to serve as a valid reference, we derive weighted seasonal averages (DJF, MAM, JJA, SON) from the monthly means, and 10° weighted  $\Delta\varphi_{EQ}$  means from the 5°  $\Delta\varphi_{EQ}$  means. Additionally, we calculate the weighted mean across all 1 K  $\Delta T$  and 10 ppbv  $\Delta O_3$  ranges. In this averaging process, each bin is weighted based on the number of CARIBIC flights ( $N_{\text{fl}}^{\text{CA}*}$ ) that contribute to the mean values (see Eq. 1) in every 1 K  $\Delta T$ , 10 ppbv  $\Delta O_3$ , 5°  $\Delta\varphi_{EQ}$ , and monthly range:

$$225 \quad \overline{\text{RH}}_{\text{liq}} = \frac{1}{N_{\text{fl}}^{\text{CA}}} \sum_{i=0}^n \overline{\text{RH}}_{\text{liq}}^*[i] \times N_{\text{fl}}^{\text{CA}}[i], \quad \text{with} \quad N_{\text{fl}}^{\text{CA}} = \sum_{i=0}^n N_{\text{fl}}^{\text{CA}*}[i], \quad (2)$$

where  $n$  is the number of bins that contribute to  $\overline{RH}_{liq}$ .

This weighted averaging approach ensures that each bin is appropriately represented in the final intercomparison, taking into account the relatively small number of flights available in the CARIBIC data set compared to MOZAIC&CORE. For instance, in the calculation of seasonal means from the respective monthly means, a higher number of flights during a particular month  
230 by CARIBIC compared to MOZAIC&CORE could lead to an over-representation of that month in the CARIBIC seasonal mean, affecting the overall intercomparison results. Since  $H_2O$  in the extratropical UT/LMS exhibits non-negligible variations on a monthly scale (Zahn et al., 2014; Kunz et al., 2008), this weighting is crucial to ensure ~~a fair~~ an appropriate comparison between the datasets and to obtain reliable and meaningful results. Overall, this approach was found to significantly improve the accuracy of the statistical comparability of the datasets.

235 By applying the mapping approach described above, sampling bins that contain too few flights are excluded, as these could lead to higher uncertainties due to the natural variability of  $H_2O$  in the UT/LMS despite the use of the geophysically-based coordinate system. This uncertainty is expected to decrease with height above the tropopause, as has been shown for  $H_2O$  based on the calculation of a trade-off factor between including more measurements versus adding more geophysical variability (due to year-to-year or longitudinal variations). This trade-off factor shows that ~~much less~~ fewer measurements are needed  
240 to constrain the mean  $H_2O$  value in a certain bin the higher above the tropopause it lies (Hegglin et al., 2008), providing confidence to our approach ~~taken~~. Thus, the minimum number of flights required for a sampling bin to be included in the final intercomparison varies with the height relative to the TTP. Specifically, the minimum number of flights linearly decreases from 15 in the lowest vertical range below the TTP (-1 to -0.75 km) to 4 flights at 3 km and higher above the TTP.

Despite the relatively limited number of flights available in the CARIBIC data set, a considerable number of sampling bins  
245 ( $\Delta z_{TTP} = 0.25$  km,  $\Delta \varphi_{EQ} = 10^\circ$ ,  $\Delta \tau_{season}$ ) contain a sufficient number of data and flights through the years to represent the multi-annual climatological state and thus enable a reliable intercomparison with MOZAIC&CORE (as detailed in Section 3.3).

### 3.2 Intercomparison of IAGOS-CARIBIC and JULIA $H_2O$

$H_2O$  data from CARIBIC serve as a reference for evaluating the extensive dataset of MOZAIC&CORE. To ensure the high  
250 quality of the CARIBIC data, the performance of the CARIBIC  $H_2O$  measurements (combination of WaSul and FPH; see Section 2.1.2 and (Zahn et al., 2014)) is validated by comparison with high precision instruments, such as FISH, compiled in the research aircraft data set JULIA (Section 2.1.3). In the past, joint flights of the WaSul sensor and the FISH hygrometer were conducted, enabling a direct comparison of  $H_2O$  measurements from both instruments (Meyer et al., 2015; Tatrai et al., 2015; Rolf et al., 2023). While notable differences outside the expected noise level were observed between the two instruments  
255 in dry stratospheric air masses of 10 ppmv and less, no systematic bias in either the dry or wet direction was identified (Tatrai et al., 2015). ~~However, because of the additional operation of an FPH, further investigation is needed to assess the agreement between CARIBIC and JULIA  $H_2O$  in the LMS.~~

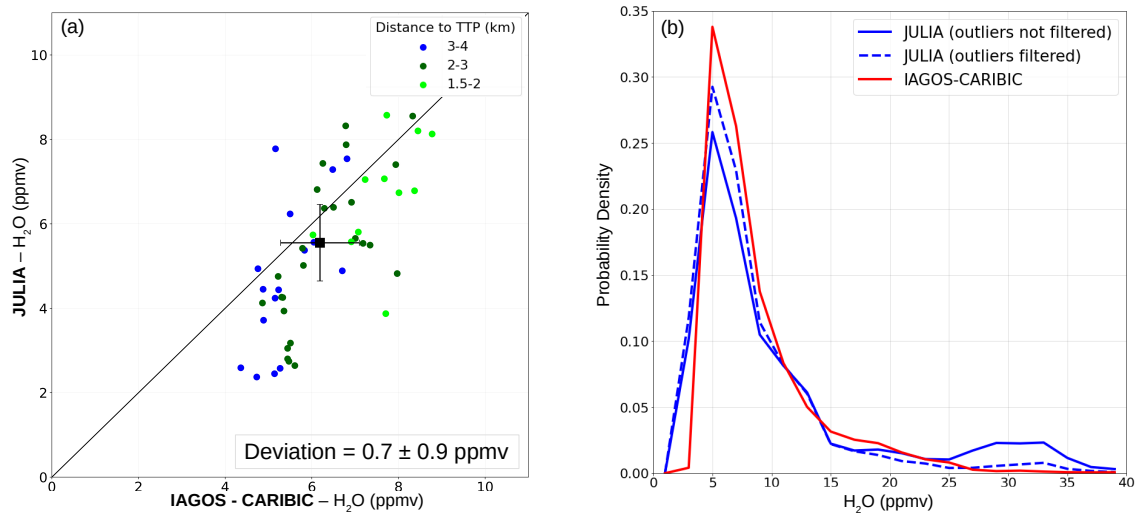


**Figure 4. Statistical intercomparison of IAGOS-CARIBIC with JULIA H<sub>2</sub>O.** (a) LMS H<sub>2</sub>O mixing ratios of IAGOS-CARIBIC versus JULIA, calculated based on the methodology described in Section 3.1 and 3.2; the color code denotes the distance to the TTP (see legend). The mean bias and the corresponding standard deviation based on all sampling bins is indicated by the black dot and the bar, respectively. (b) Based on single measurements from all sampling bins in (a), the frequency distribution is shown both with and without the filtering of strong outliers.

### 3.2.1 Preparation of the datasets

For the comparison of CARIBIC and JULIA H<sub>2</sub>O data in the LMS, the binning strategy described in Section 3.1 and depicted in Figure 3 is employed. In the comparison, only sampling bins at distances of at least 1.5 km above the TTP are ~~taken~~included. This reduces the impact of the natural H<sub>2</sub>O variability ~~in~~on the comparison, which is higher close to the TTP and in the UT; ~~thereby improving the accuracy and reliability of the results.~~

The higher sampling altitude of JULIA results in the sampling of different air masses, which might correspond to different H<sub>2</sub>O concentrations, compared to CARIBIC. Therefore, we only consider CARIBIC and JULIA measurements between 10.5 and 12.5 km and a mean height difference below 0.5 km between the respective sampling bins to ensure consistency. ~~Moreover~~Additionally, in our data sampling process, we use potential temperature instead of temperature, ~~to~~to further reducing the effect of the natural H<sub>2</sub>O variability.

The JULIA data are subjected to a filtering criterion that excludes cases with RH<sub>ice</sub> values larger than 80 % (see Section 2.1.3). This criterion is applied because the JULIA data include total water (=gas phase + cloud ice particles). Using values below 80 % RH<sub>ice</sub> ensures that in-cloud measurements are excluded. For consistency in the comparison, we also exclude RH<sub>ice</sub> values above 80 % in the CARIBIC data set.

Last, but not least, to reduce the influence of strong outliers, CARIBIC and JULIA sampling bins are excluded from the mean H<sub>2</sub>O values derived according to Equation 1, if the difference between the sampling bins is 10 ppmv or higher. Such deviations

are beyond the expected error range in the LMS (Tatrai et al., 2015) and likely stem from varying atmospheric conditions during the respective measurements, resulting in notable differences in H<sub>2</sub>O.

### 3.2.2 Intercomparison

The final statistical comparison of the CARIBIC and JULIA H<sub>2</sub>O datasets with all criteria described in Section 3.2.1 applied, is shown in Figure 4 (a), where each point represents one sampling bin. The mean values and corresponding standard deviations of all bins are indicated by the square ~~dot and the error bars~~ symbol and related error bars, respectively. The comparison shows a scattering of the sampled mean H<sub>2</sub>O values along an ideal regression line, but, on average over the full 0-10 ppmv range, a good agreement, with a mean difference of CARIBIC compared to JULIA of  $(0.7 \pm 0.9)$  ppmv. The scattering might be attributed to the limited amount of data from both products and the potential over-representation of anomalous atmospheric conditions in the JULIA H<sub>2</sub>O data, despite the efforts to filter out strong outliers. Figure 4 (b) displays the probability density function (PDF) based on all bins given in panel (a). Without the filtering, a significant amount of anomalously high H<sub>2</sub>O is present in the JULIA data base, which are mostly filtered out with this approach (blue dashed line) while for CARIBIC, this filtering approach does not cause significant differences (thus, only filtered data displayed in Figure 4b).

Systematic differences can be found for sampling bins where JULIA indicates H<sub>2</sub>O of less than 6 ppmv. Bins with JULIA indicating H<sub>2</sub>O of less than ~~3 ppmv occurred during the winter season in~~ 3.5 ppmv are related to polar air masses ~~with very low cold point tropopause temperatures during one specific campaign, POLARCAT (Polar Study using Aircraft, Remote Sensing, Surface Measurements and Models, of Climate, Chemistry, Aerosols, and Transport; reference missed)~~. It is not unlikely that these are cases of ~~anomalously unusually~~ low H<sub>2</sub>O that were purposefully measured during certain campaign flights and meteorological conditions, and are thus over-represented in JULIA. ~~However, it~~ When filtering out data from that specific campaign, the bias between the two datasets gets less pronounced. However CARIBIC data are still moister by 0.5 to 1 ppmv for mixing ratios below 6 ppmv (see all bins with JULIA indicating >3.5 ppmv in Figure 4a) which is outside the stated uncertainty of the JULIA and CARIBIC data (see 1). It cannot be argued whether this small mean deviation is a result of different atmospheric sampling strategies between campaign and commercial aircraft flights, despite the strict filter conditions, or a small systematic bias. Nevertheless, the ~~discrepancies shown in b are within the known uncertainties of possibility of a moist bias at the very dry end must be considered in the H<sub>2</sub>O instruments used in CARIBIC and JULIA flights (Table 1) and thus the CARIBIC H<sub>2</sub>O data are suitable for the comparison with~~ comparison between CARIBIC and MOZAIC&CORE, ~~as described which is presented~~ in the next section.

### 3.3 Evaluation of IAGOS-MOZAIC&CORE H<sub>2</sub>O

Figure 5 displays the intercomparison of the sampled mean values  $\overline{RH_{liq}}$ ,  $\overline{RH_{ice}}$ , and  $\overline{H_2O}$  (Egu. 2) with respect to the season and the distance to the tropopause. Additionally, Figure A1 shows the same plots, but the data being sampled into 5 K means instead of being averaged over all temperature ranges. MOZAIC and CORE are ~~regarded treated~~ separately to examine the agreement between them. A majority of the measurements contributing to the sampled mean values originate from the extratropics between 30 and 80°N for which this intercomparison is valid ~~for~~. For the reference dataset CARIBIC, in

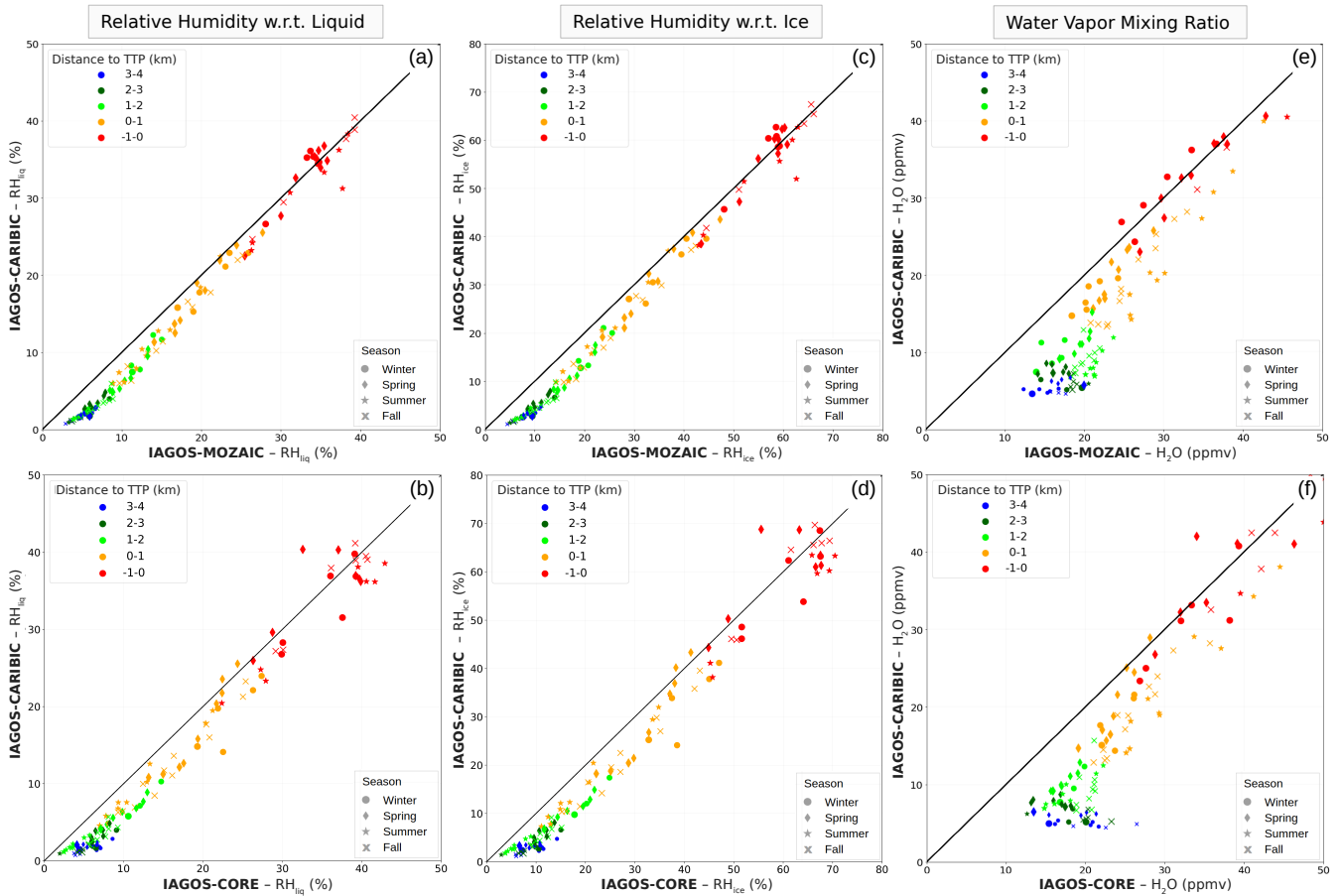


**Figure 5. Statistical intercomparison of  $\text{H}_2\text{O}$  from IAGOS-MOZAIC&CORE with IAGOS-CARIBIC .** Sampling bin means of  $\overline{\text{RH}}_{\text{liq}}$  (left column),  $\overline{\text{RH}}_{\text{ice}}$  (middle column) and  $\overline{\text{H}_2\text{O}}$  (right column) for IAGOS-MOZAIC (top) and IAGOS-CORE (bottom) versus IAGOS-CARIBIC. The sampling bins are derived following the methodology described in Section 3.1; the color code denotes the distance to the tropopause, the symbols the corresponding season.

the uncertainty of  $\overline{\text{RH}}_{\text{liq}}$ ,  $\overline{\text{RH}}_{\text{ice}}$ , uncertainties of  $\text{H}_2\text{O}$  (4 %), temperature (0.7 K; Benjamin et al. (1999)) and pressure (1 hPa; Tang et al. (2005)), incorporate. The resulting relative bias of the CARIBIC sampling bins is on the order of 7 %.

In the comparison of MOZAIC to CARIBIC data, a distinct relationship is observed. When examining bins below the TTP where  $\overline{\text{RH}}_{\text{liq}}$  values are mostly above 30 %, MOZAIC and CARIBIC show a good agreement. This agreement is attributed to the infrequent occurrence of dry conditions with low  $\text{RH}_{\text{liq}}$  values of 10 % and less, which tend to be biased (Neis et al., 2015a) and therefore do not significantly impact the mean values in this height range. Figure 6a illustrates the correlation between the relative number of MOZAIC measurements below 10 %  $\text{RH}_{\text{liq}}$ , which was stated to be the upper limit for which ICH data shows good quality by Neis et al. (2015a), and the bias between MOZAIC and CARIBIC. For MOZAIC and CARIBIC, b  
 315 displays the PDFs from all measurements that fall within the 0 – 10 % and 10 – 20 %  $\overline{\text{RH}}_{\text{liq}}$  ranges of MOZAIC in a. Notably,

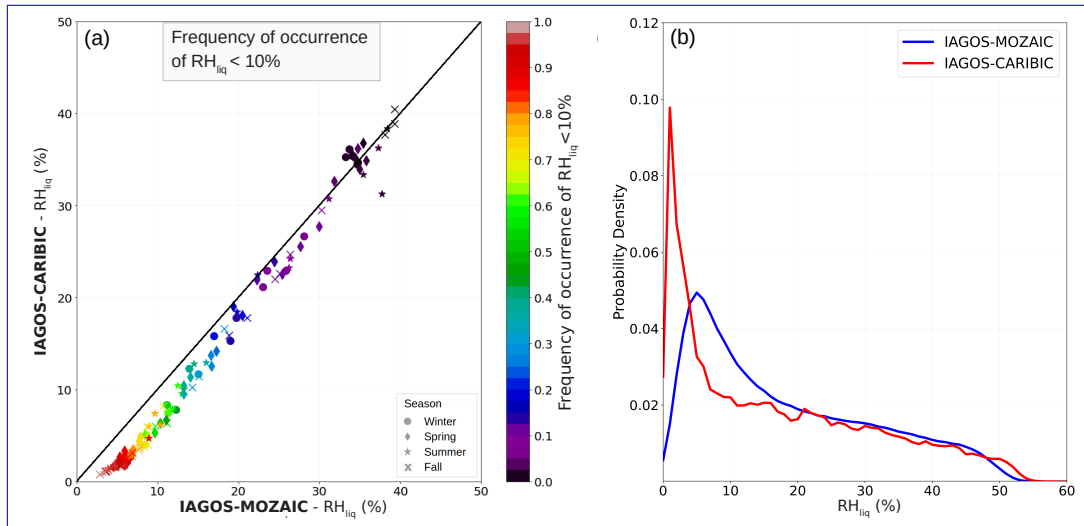


**Figure 6.** (a) For IAGOS-MOZAIC, the plots show the same sampling bins as in Figure 5. The color code indicates the frequency of occurrence of single measurements below a threshold of 10% by IAGOS-MOZAIC that contribute to the shown mean values. (b) For all bins in with  $\overline{RH_{liq}}$  of 0-10% and 10-20%, the corresponding occurrence frequencies of  $RH_{liq}$  measurements is shown for IAGOS-MOZAIC-CARIBIC and -CARIBIC-MOZAIC, based on all data that go into the sampling bins in (a).

the bias is prominent when the amount of measurements below 10 %  $RH_{liq}$  is higher than 20 % (Figure 6a), while bins with fewer measurements below 10 %  $RH_{liq}$  show little to no significant biases. This correlation pattern is also observed for CORE (not shown). However, it cannot be verified from our analyses where the upper limit is situated above which the measurements are of good quality.

320 For MOZAIC and CARIBIC, Figure 6b presents the PDFs constructed from all measurements included in the sampling bins of Figure 6a. The PDFs in panel (b) exhibit a similar pattern for  $RH_{liq}$  values above 20 %, but they diverge significantly below this threshold, suggesting that ICH  $RH_{liq}$  might be biased for values under 20 %. However, the observed discrepancy in the  $RH_{liq} > 10\%$  range could also reflect a scenario where no consistent bias exists across specific  $RH_{liq}$  ranges. Instead, a broad distribution of measurements around a biased mean state may be present. In such a case, a mean moist bias for a given  $RH_{liq}$  range would increase the PDF's representation of  $RH_{liq}$  values at higher levels.

325 Non-linear bias behavior could be attributed to uncertainties in the calibration the sensor's offset drift, which occurs between the routine ICH calibrations conducted every three months (Petzold et al., 2020). Although an in-flight calibration is performed to account for this sensor drift (Smit et al., 2008), uncertainties in the process (as noted in Smit et al. (2008)) can introduce non-linear variations in the bias of individual measurements between calibration intervals. Consequently, while this intercomparison study cannot determine the behavior of the bias for individual measurements, it does provide insights into the bias of mean values used in climatological studies.

330 The sampling bins with  $\overline{RH_{liq}}$  values below 20 % exhibit significant systematic moist biases, with relative differences of 100 % or more for  $\overline{RH_{liq}}$  of 10 % and less. For layers closer to the TTP, there is a lower but still noteworthy bias. During

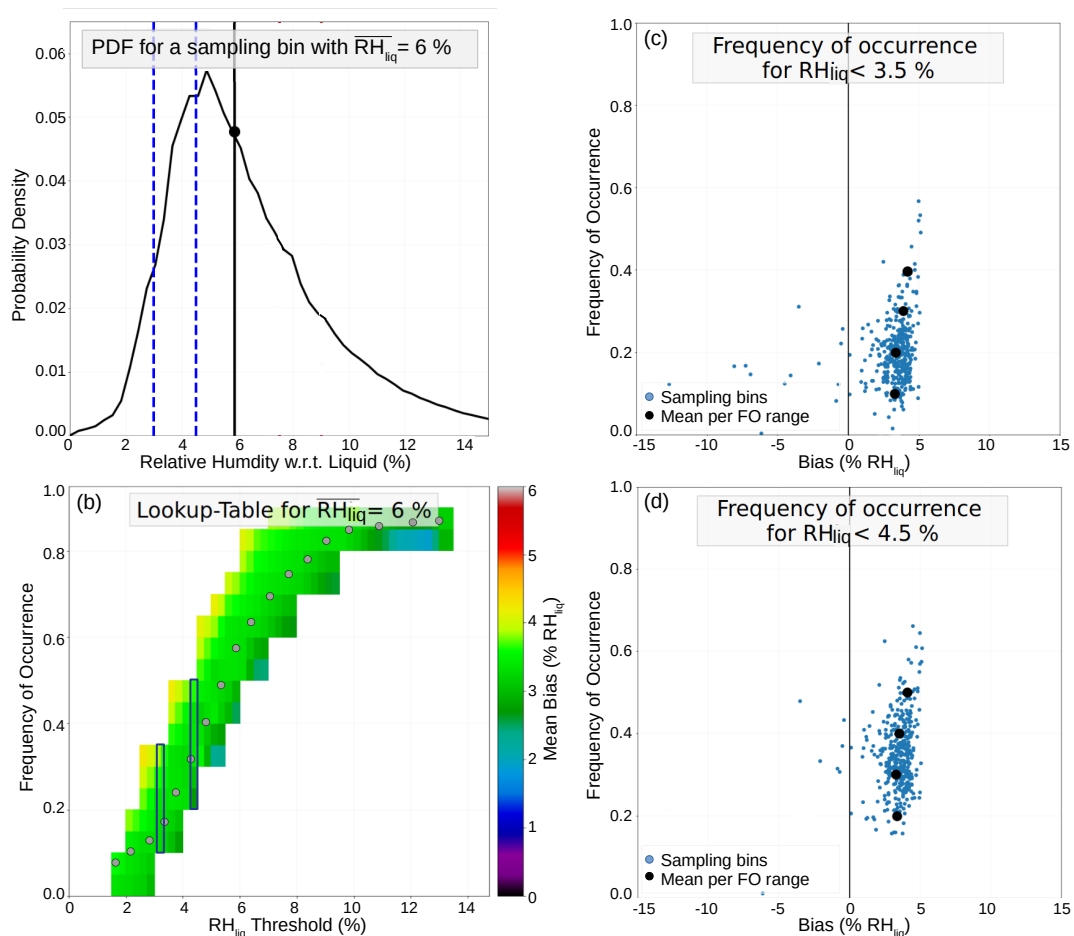


**Figure 7. Application example of the IAGOS adjustment algorithm.** (a) Example  $RH_{liq}$  frequency distribution of a sampling bin with a mean of  $\overline{RH_{liq}} = 6\%$ . For this mean value, (b) shows the lookup-table with the values used as adjustment based on different  $RH_{liq}$  thresholds and the corresponding frequency-of-occurrences-cumulative-distribution (FOs y-axis). For the two thresholds indicated by the blue dotted lines in (a), the plots (c) and (d) exemplary show the derivation of the mean bias (black dots) based on the weighted mean of the sampled mean values (blue dots).

summer, certain bins have  $\overline{RH_{liq}}$  values of 15 % or less already in the first kilometer above the TTP, whereas the same levels  
 335 relative to the TTP during other seasons indicate much higher values. This seasonality is attributed to the higher temperatures  
 observed in the respective sampling bins during the summer season. Conversely, in the winter season, a considerable number  
 of MOZAIC&CORE measurements in the lowest kilometer above the TTP are higher than 10 % (as shown in a), thereby  
 providing more reliable mean values. Consequently, and biases of the mean values are in the range of only about 1 to 3 %  
 $RH_{liq}$  during this season close to the TTP.

340 For the comparison of CORE and CARIBIC, we used data between 2018 and 2022 only. This specific time frame was chosen

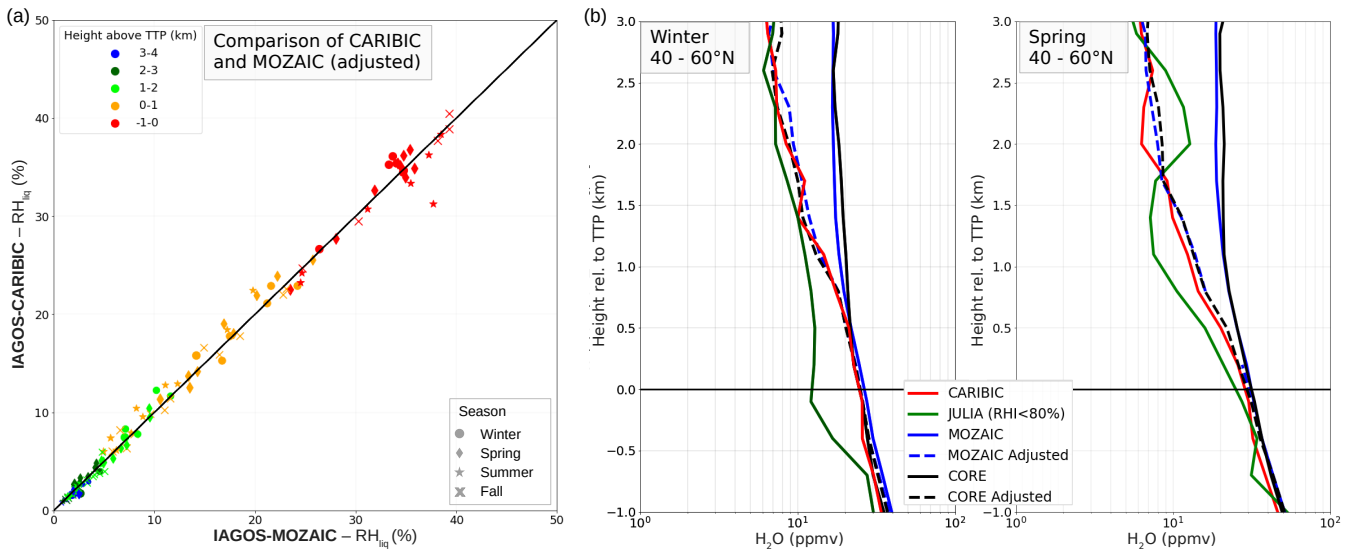


**Figure 8. Application of the adjustment algorithm on the IAGOS data.** Panel (a) shows a comparison of the same sampling bins between IAGOS-MOZAIC and IAGOS-CARIBIC as shown in Figure 6 but with the adjustment algorithm applied to the mean values. Panel (b) shows two mean vertical UT/LMS H<sub>2</sub>O profiles of IAGOS-CARIBIC, JULIA, and IAGOS-MOZAIC&CORE (adjusted and unadjusted).

because before 2018, a ~~systematic failure of the temperature sensor at the humidity capacity sensor occurred. Although the resulting error was adjusted afterwards~~ grounding issue between the sensor and the data acquisition unit caused a large noise on the signal and thus a reduced quality flag of the data. Therefore, we decided to utilize only data with the highest quality unaffected by this issue, ~~to ensure that no systematic biases affect the analysis.~~

345 On average, the comparison of CORE and CARIBIC shows similar mean biases in the LMS, similar to what the comparison with MOZAIC revealed. However, for CORE, there is a stronger variation of the bins bin mean values compared to MOZAIC, which can be attributed to differences in the temporal coverage (2018-2022 and 1995-2022 ~~for~~) of CORE and CARIBIC, respectively, due to the large year-to-year variability of UT/LMS H<sub>2</sub>O (Kunz et al., 2008).

#### 4 ~~Adjustment of IAGOS-MOZAIC&CORE LMS H<sub>2</sub>O to IAGOS-CARIBIC~~

350 4 Adjustment of IAGOS-MOZAIC&CORE LMS H<sub>2</sub>O to IAGOS-CARIBIC

##### 4.1 Adjustment methodology

~~Based on Following~~ the mapping approach ~~used to make the different H<sub>2</sub>O data sets comparable (Section 3.1) outlined in Section 3.1,~~ the next step is to apply an ~~adjustment algorithm to~~ algorithm to adjust the biased MOZAIC&CORE H<sub>2</sub>O data, using CARIBIC H<sub>2</sub>O as ~~reference. For a reference. A fixed bias for individual measurements, a fixed bias however, cannot be~~ defined as a function of RH<sub>liq</sub> ~~cannot be determined. This is~~ due to the sensor offset drift at 0 % RH<sub>liq</sub> ~~that occurs between~~

355

the ICH calibrations, which are conducted every three months (Petzold et al., 2020). An in-flight calibration is used to adjust this sensor shift (Smit et al., 2008), but uncertainties in the in-flight calibration (as discussed in Smit et al. (2008)) may cause a nonlinear behavior in the bias of single measurements as a function of  $RH_{liq}$  between the calibrations. Consequently (see Section 3.3). As a result, it is also not feasible to directly use data from campaign flights adjust ICH data from IAGOS flights using data from campaign flights equipped with ICH and high-precision H<sub>2</sub>O instruments like FISH to adjust ICH data measured onboard IAGOS flights, like FISH.

Because of the reasons Given the limitations mentioned above, the primary objective is to focus on adjusting of our methodology is to adjust the sampling bin mean values  $\overline{RH_{liq}}$  (Section 3.3), which consist of a large number of measurements in the order of several thousand that. These mean values, based on thousands of individual measurements, represent a climatological state. One approach would be to fit the PDFs of. One potential approach is to align the probability density functions (PDFs) of the MOZAIC&CORE to the ones data with those of the reference dataset, CARIBIC (CARIBIC); see Figure 6b for illustration. However, because of a relatively small number of CARIBIC data, the corresponding PDFs of the CARIBIC CARIBIC has fewer measurements, the PDFs for its sampling bin mean values (i.e. the ones shown in ) are often not smooth, in contrast to the smoother distributions observed in the MOZAIC&CORE dataset. This disparity poses a challenge when attempting to fit the PDFs straightforwardly. To address this issue, are noisier and more variable, making it difficult to directly match the distributions. As a result, we pursue an alternative approach is adopted, which is described below. For every sampling bin according to Equation 1, each of the corresponding: analyzing how the probability distribution function of the data influences the mean bias, and adjusting accordingly. The steps of the approach are described below:

1. **Segmenting the distribution and analyzing the bias by frequency of occurrence (FO):** We divide the  $RH_{liq}$  frequency distributions is sliced into distribution of each sampling bin into smaller segments. For every of these segments, each segment, we compute the frequency of occurrence (FO) of measurements values falling below specific  $RH_{liq}$  thresholds (FO thresholds is derived, i.e.  $FO = \sum_{ii=0}^{RH_{liq}^{thres.}} PDF_{ii}$ , as shown 0.5 - 15 %  $RH_{liq}$ , with step size of 0.5 %). This allows us to determine how often certain  $RH_{liq}$  values occur in the distribution. As an example, in Figure 6a, the FO for the 10 % threshold in a. This principle is illustrated in is shown. Figure 7a for one specific  $RH_{liq}$  illustrates this concept for a distribution having a mean  $\overline{RH_{liq}}$  of 6 %, with the blue lines indicating two specific  $RH_{liq}$  thresholds,  $RH_{liq} < 3.5\%$  and  $RH_{liq}$  PDF with a sampling mean value of  $\overline{RH_{liq}} = 6\%$ . For all  $< 4.5\%$ .

We perform this segmentation for the distributions of all MOZAIC&CORE sampling bins that fall within the range 5.5 to 6.5 in between certain  $\overline{RH_{liq}}$  ranges, with a step size of 1 %  $RH_{liq}$ , c and d illustrate the FO of two specific thresholds ( $\sum FO$  for  $RH_{liq} < 3\%$  and  $< 4.5\%$ ) and the respective biases of MOZAIC compared to CARIBIC. Again, MOZAIC and CORE were treated separately but the results also account for CORE. The corresponding mean  $\overline{RH_{liq}} = 0.5 - 1.5\%$ , 1.5 - 2.5 %, ...). For each of the bins in the respective  $\overline{RH_{liq}}$  ranges, the bias to the CARIBIC sampling bins is calculated. Next, we also consider the different FO thresholds and sort the biases as a function of the FO (dashed regression lines in amount of measurements falling below these thresholds. For the two  $RH_{liq}$  thresholds indicated in Figure 7e,d) exhibit a robust relation with the FO, and the variations along the bias regression line are within  $\pm 0.5\%$   $RH_{liq}$ . For  $\overline{RH_{liq}} = 6\%$ , a broader distribution, i.e. a higher FO for the two thresholds shown in a (blue dashed lines), and based on all sampling

bins with  $\overline{RH}_{liq}$  in the range of 5.5 – 6.5 %, Figure 7c and d, correspond to a higher bias & displays the respective biases as a function of the FO (y-axis) is shown (blue dots). Similar plots like the ones in , but for a mean value of for  $\overline{RH}_{liq} = 15 \%$  , are presented in Figure A2.

By performing this approach for certain  $\overline{RH}_{liq}$  ranges, like it was done for the 5.5 – 6.5 % range, the mean biases as a function of the respective FOs are calculated. Furthermore, a moving average step size of 0.25

395

2. **Derivation of a mean bias as a function of  $\overline{RH}_{liq}$  and FO:** A regression (black dots in Figure 7c&d) is applied to the correlation between all biases and FO fulfilling the  $RH_{liq}$  threshold. The deviations from the regression are on the order of  $\pm 0.5 \%$   $RH_{liq}$  is applied for  $\overline{RH}_{liq}$ , e.g. 5.5 – 6.5 %  $\overline{RH}_{liq}$  and thus a robust approximation. By performing this method for various ranges of  $\overline{RH}_{liq}$ , 5.75 – 6.75 %  $\overline{RH}_{liq}$ , and so on. Using this approach, we obtain the mean biases  $\Delta RH_{liq}$ , a series of mean biases as a function of (1) ranges of  $\overline{RH}_{liq}$  values, and (2) both %  $RH_{liq}$  thresholds and the corresponding FOs. Subsequently FO. This enables us to study how the bias varies as a function of the distribution of data points.

400

3. **Interpolation and Construction of Lookup Tables for Bias Correction:** Once the mean biases (black dots) for different FO thresholds are calculated, we apply interpolation to the mean deviations between various ranges of average  $\overline{RH}_{liq}$  values to mitigate fluctuations stemming from uncertainties in the  $RH_{liq}$  distribution. This approach yields an interpolation to smooth the fluctuations between the bias values for different  $\overline{RH}_{liq}$  ranges. This step is necessary to minimize the effects of distribution uncertainties, leading to more consistent and reliable corrections. The result is a set of comprehensive lookup tables containing the mean deviations for specific average  $\overline{RH}_{liq}$  lookup tables containing the corrected mean values for specific  $\overline{RH}_{liq}$  values and the respective corresponding FO thresholds. An illustrative example of such a lookup table for  $\overline{RH}_{liq}$  lookup table for  $\overline{RH}_{liq} = 6\%$  is presented in Figure 7b. The two black boxes correspond to the biases of % is shown in Figure 7b, where the black boxes highlight the biases corresponding to the two thresholds shown in 7c and Figure 7c&d.

405

410

In the final adjustment, the

415

4. **Final Bias Calculation and Adjustment:** The final adjusted mean bias is derived from by calculating the arithmetic mean of the biases indicated by at different FO thresholds. The equation for the final mean bias is given by:

$$\overline{\Delta RH}_{liq} = \frac{1}{n} \sum_{i=0}^n \Delta RH_{liq}[i], \quad (3)$$

with n where n represents the number of FO thresholds. As an example, for the distribution shown in a, the the biases for different  $RH_{liq}$  FO thresholds are represented by the black line illustrated by the grey dots in Figure 7b. To obtain the The final mean bias,  $\overline{\Delta RH}_{liq}$ , the arithmetic mean of all these individual biases is calculated is obtained by averaging all the individual biases. This approach ensures that we consider and incorporate account for the biases associated with various FO thresholds, leading to a more comprehensive and accurate assessment adjustment of the mean bias for the specific mean value  $\overline{RH}_{liq}$ . Applying  $RH_{liq}$  values.

420

When the adjustment algorithm described in this section is applied to the entire MOZAIC data set, i.e. dataset, using the sampled mean values shown in Figure 5, the corrected values exhibit a good agreement to with the CARIBIC data can now be found, as can be seen, as shown in Figure 8a, where the sampled  $\overline{RH_{liq}}$  are closely distributed. The adjusted MOZAIC values now cluster closely around the 1-to-1 line without, without any obvious bias. Furthermore, Figure 8b illustrates two examples of vertically resolved mean presents vertical profiles of  $H_2O$  from MOZAIC (blue) & CORE (black) (both not adjusted, solid lines, and adjusted, dashed lines) as well as, CARIBIC (red), and JULIA (green) during the winter and spring seasons in the 40–60°N latitudinal region. At heights of 1 km altitudes of 1 km and more above the TTP (depending on the season), where MOZAIC & CORE exhibit exhibited significant biases, the adjusted mean values now reveal a good agreement with JULIA and CARIBIC within the expected variation range. This outcome signifies align well with the reference data (CARIBIC and JULIA). This confirms that the adjustment methodology is effective and provides reliable mean values independent of the season. For JULIA, lower values compared to CARIBIC, MOZAIC, and CORE in the lowest 1 km above the TTP can be explained by the filtering of mean  $H_2O$  values that correspond to ice relative humidity higher than 80% to avoid sampling bins containing ice particles (as described in Section 2.1.3) across different seasons.

## 4.2 Application and uncertainties of adjusted IAGOS-MOZAIC & CORE $H_2O$

The adjustment of the MOZAIC & CORE-based  $H_2O$  climatologies offers the advantage of resolving spatial and seasonal variability at a higher resolution than would be possible with just the in-situ data sets of CARIBIC and JULIA. The adjustment of mean values requires a sufficient number of measurements, in order to provide a smooth PDF based on which the adjustment is performed. In the lower stratosphere (LS), variability in  $H_2O$  increases with altitude towards the tropopause, necessitating a larger number of measurements to ensure the PDF is not skewed by outliers. To determine the necessary number of measurements, a Kolmogorov-Smirnov test (Berger and Zhou, 2014) is performed. This test assesses whether the data fits a specific distribution, typically a Weibull distribution for the IAGOS-

### 4.2.1 Uncertainty estimate

While the adjustment improves the agreement between the MOZAIC & CORE and CARIBIC datasets, several sources of uncertainty remain. These include:

- **Measurement uncertainties:** In CARIBIC, uncertainties in the  $RH_{liq}$  data, with at least 95% confidence. For the sampling strategy outlined in this study (Section 3.1), the required number of data points ranges from approximately 300 (LMS;  $\Delta z > 2$  km) to 1000 (UT). Despite the good agreement as shown in , one has to keep in mind that for the resulting adjusted MOZAIC & CORE  $\overline{H_2O}$ , uncertainties due to (1) measurement uncertainties and (2) uncertainties in the adjustment itself incorporate. For the CARIBIC measurement uncertainty, in the derivation of  $RH_{liq}$ , uncertainties of derivation (from  $H_2O$  (4%), temperature (0.7 K; Benjamin et al., 1999) and pressure (1 hPa; Tang et al., 2005), are taken into account. The resulting relative bias in the error propagation is in the order of, temperature, and pressure

455 ~~measurements) introduce a relative bias of about 7 %. The uncertainty due to limitations in the method results from the~~  
~~% (see Section 3.2.2).~~

– ~~**Method uncertainty:** The small number of CARIBIC data measurements and differences in the temporal coverage~~  
~~between the products, with H<sub>2</sub>O showing a large year-to-year variability in the LMS (Kunz et al., 2008). Furthermore,~~  
460 ~~differences in the geographical coverage might also induce uncertainties, despite that the sampling strategy should~~  
~~strongly decrease uncertainties in the comparison due to this reason, and geographical coverage of the datasets can~~  
~~lead to uncertainties. However, the sampling strategy designed in this study helps reduce such uncertainties.~~

The method uncertainty is determined like the following: The bias derivation (see Figure 7) is also performed for each season separately. In the next step, the standard deviation for each bias as a function of  $\overline{RH_{liq}}$  and FO (see last section) is derived from the four seasonal means, and from these deviation, the mean standard deviation as a function of just  $\overline{RH_{liq}}$ .  
465 The mean bias (averaged over all FO) as a function of unadjusted  $\overline{RH_{liq}}$  is shown in Figure 9 (dashed line), with the red area indicating the uncertainty due to the adjustment method and the blue area the additional uncertainty when measurement uncertainties are also taken into account. The uncertainty of the derived adjusted  $\overline{H_2O}$  vary depending on the corresponding  $\overline{RH_{liq}}$ . During summer,  $\overline{RH_{liq}}$  in the LMS tend to be lower due to higher temperatures compared to winter, with lower  $\overline{RH_{liq}}$  having higher relative uncertainties. Based on all  $\overline{RH_{liq}}$  in the extratropical LMS, Figure 9b and c show the mean uncertainty  
470 and the 10 – 90 % percentile (dashed line and shaded area, respectively). For 10 ppmv for example, the mean bias (bias range) is 1.0 (0.8 – 2.3) ppmv and 2.4 (2.0 – 3.1) ppmv for winter and summer, respectively.

#### 4.2.2 Application

~~The adjusted MOZAIC&CORE-based H<sub>2</sub>O climatology offers the advantage of a longer record and greater spatial and seasonal~~  
~~sampling than the datasets of CARIBIC and JULIA, enabling more detailed analysis of the drivers of H<sub>2</sub>O variability. However,~~  
475 ~~the adjustment of mean values requires a sufficient number of measurements, in order to provide a smooth PDF based on which~~  
~~the adjustment is performed. In the lower stratosphere (LS), variability in H<sub>2</sub>O increases with altitude towards the tropopause,~~  
~~necessitating a larger number of measurements to ensure the PDF is not skewed by outliers.~~

~~To determine the necessary number of measurements, a Kolmogorov-Smirnov test (Berger and Zhou, 2014) is performed. This~~  
~~test assesses whether the data fits a specific distribution, typically a Weibull distribution for the IAGOS RH<sub>liq</sub> data, with at least~~  
480 ~~95 % confidence. For the sampling strategy outlined in this study (Section 3.1), the required number of data points ranges from~~  
~~approximately 300 (LMS;  $\Delta z > 2$  km) to 1000 (UT).~~

~~Due to the requirement for a substantial amount of data and the relative uncertainty exceeding 10 % in the driest range, robust~~  
~~trend analysis cannot be reliably performed using the derived data set. Even in regions with sufficient data availability, the level~~  
~~of uncertainty reflects the potential magnitude of H<sub>2</sub>O trends.~~

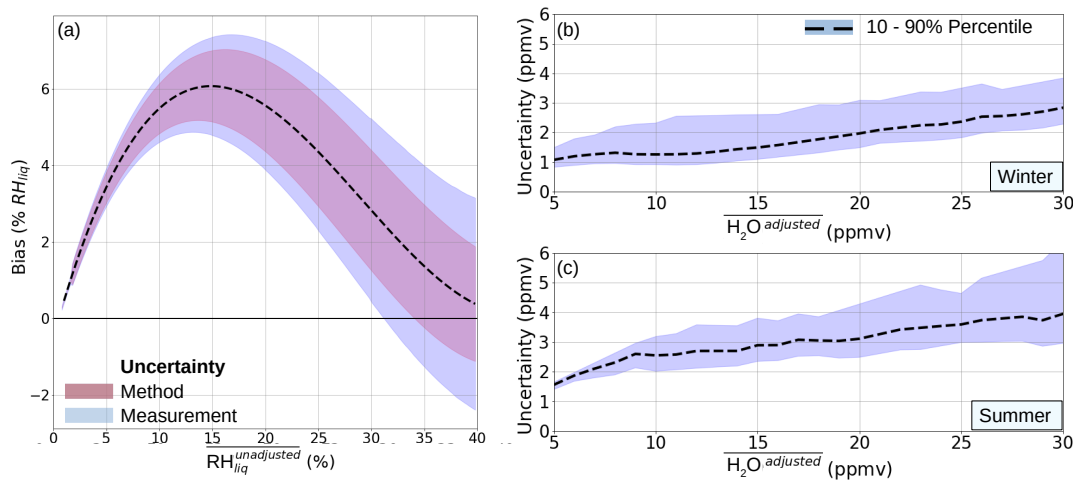


**Figure 9. Error Budget** (a) Mean bias derived from the mean of all FO thresholds as a function of  $\overline{RH_{liq}}$  (solid-dashed line) and the uncertainty estimate due to the adjustment method (red shaded) and due to measurement uncertainties (blue shaded). (b and c) For  $\overline{H_2O}$  derived from adjusted  $\overline{RH_{liq}}$ , the mean bias (dashed line) and the 10 – 90 % percentile (blue shaded) is shown for winter (b) and summer (c).

### 485 4.3 Adjusted UT/LMS H<sub>2</sub>O climatologies

Multi-annual monthly means of adjusted H<sub>2</sub>O, based on all MOZAIC&CORE data, are shown in Figure 10 for two  $\Theta$  levels, 335 K (a-d) and 350 K (e-h). The magenta solid line indicates the mean 2 PVU line. The H<sub>2</sub>O data is provided with a resolution of at least 5 ppmv. This relatively low resolution was chosen in regard of the uncertainties in the adjusted dataset. Specifically, for values below 20 ppmv, the uncertainty of the adjusted data can reach up to 30 %. Therefore, a higher resolution would not be meaningful. Nonetheless, the given resolution is sufficient to capture spatial and seasonal features, also in areas where CARIBIC data is sparse or unavailable due to limited flight coverage (see discussion below)

Over parts of N. America as well as SE. Asia, the monsoon related H<sub>2</sub>O increase during the Northern hemisphere summer season (Nützel et al., 2019) is evident at  $\Theta = 350$  K (Figure 10g), i.e. at a  $\Theta$  level that corresponds to subtropical and tropical air masses at passenger aircraft altitude over these regions. Here, mean values are by a factor of 3 (N. America) to 10 (SE. Asian) higher, compared to other regions at the same geographic latitudes.

From fall to spring the highest values in the mid-latitudes at 335 K can be found over the N. Atlantic. Higher H<sub>2</sub>O amounts occur over the Atlantic than over continental regions during the winter half of the year, ~~higher compared to the continental regions, correlate with the high associated with greater~~ low pressure activity over this area, and the resulting large scale uplift of moist and relatively warm air masses (UT) and potential isentropic mixing of moisture into the LS. Enhanced isentropic mixing into the LS over the Atlantic was found to occur in relation to warm conveyor belt outflow (Kunkel et al., 2019), based on measurements during the WISE (Wave-driven ISentropic Exchange) campaign.

For the N. Atlantic (50 - 70°N and 5 - 65°W), Figure 11 a-d show adjusted  $\overline{H_2O}$  climatologies, given in coordinates of equivalent latitude and potential temperature difference relative to the TTP ( $\Delta\Theta$ ). Close to the TTP ( $\pm 20$  K), a strong annual H<sub>2</sub>O cycle

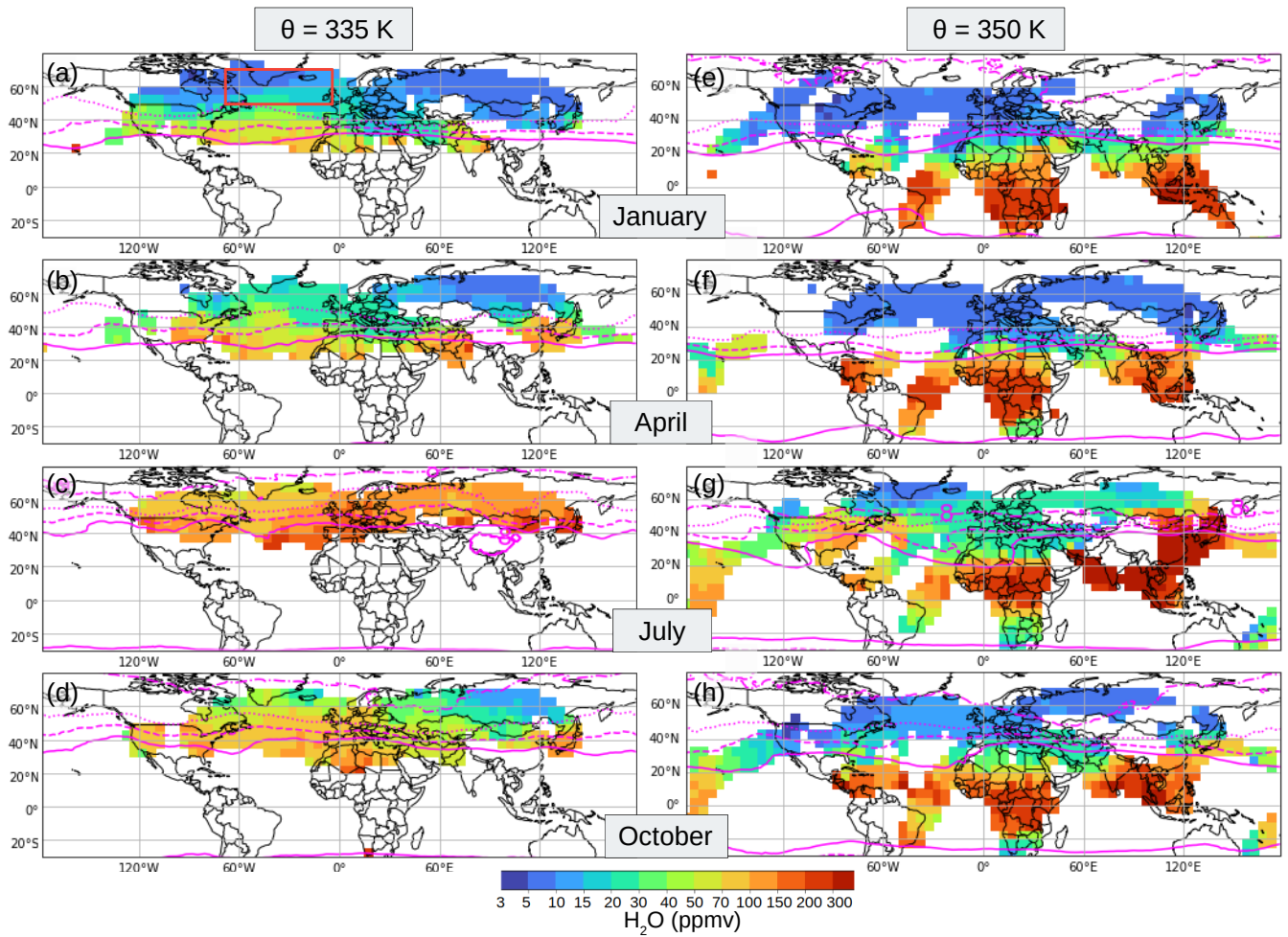


**Figure 10.**  $\text{H}_2\text{O}$  mixing ratio climatologies. Monthly means (January, April, July and October) for two  $\Theta$  level. In magenta, solid, dashed, dotted, and dash-dotted, the mean position of the 2, 4, 6 and 8 PVU line is indicated. [The red box in \(a\) highlights the region further investigated in Figure 11](#)

can be observed. Along the TTP, the  $\text{H}_2\text{O}$  varies between 20 to 30 ppmv (winter;  $\Theta = 315\text{K} - 325$ ), and  $\sim 100$  ppmv (summer;  $\Theta = 325 - 340$  K). Investigating the annual cycle along isentropic levels in the LMS, at 340 K, a distinct increase during the summer half of the year can be found. During January,  $\text{H}_2\text{O}$  is in the range of 5 -  $\sim 20$  ppmv and increases to 15 - 70 ppmv during July, with a strong gradient along  $\Delta\varphi_{\text{EQ}}$  ranges, [indicating the potential isentropic](#). [This pattern can strongly be related to the increase of the tropopause  \$\Theta\$  level during summer and the subsequently stronger influence of \(isentropic\) transport of  \$\text{H}\_2\text{O}\$  from the subtropical regions into the mid-latitudinal LMS.](#) At 350 K, the annual cycle is less pronounced compared to the levels below, with a variation from mostly 5 - 7 ppmv along all  $\Delta\varphi_{\text{EQ}}$  during winter, to an increase to 15 - 20 ppmv during summer in the southernmost  $\Delta\varphi_{\text{EQ}}$  range covered (40 - 50°N). [mid-latitude LMS. Generally, layers in](#)

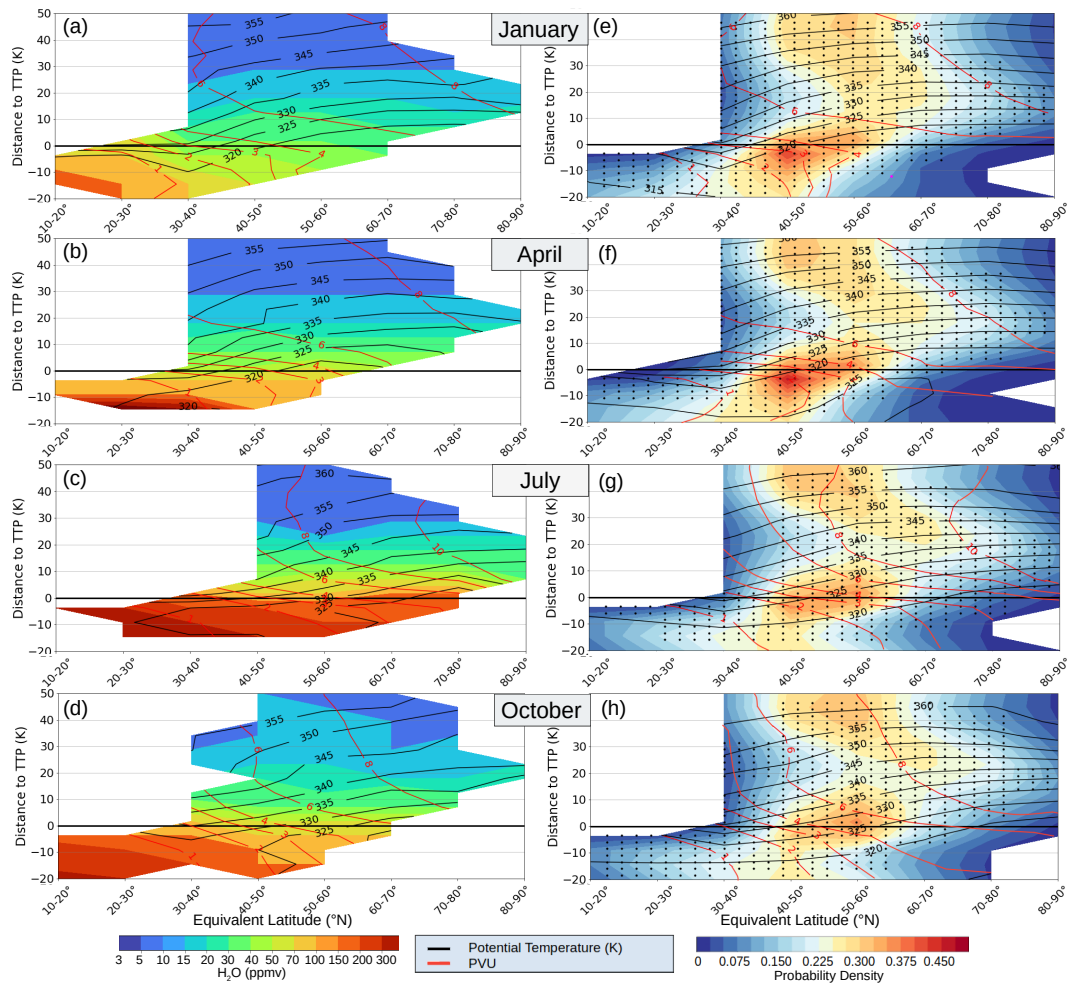


**Figure 11. Adjusted UT/LMS H<sub>2</sub>O mixing ratio climatology for the North Atlantic region (50-70°N and 5-65°W).** (a-d) show the multi-annual monthly means of the adjusted H<sub>2</sub>O. (e-h) Occurrence frequency of sampling bins of equivalent latitude and potential temperature difference ( $\Delta\Theta$ ) to the TTP (the resolution is 5 K and normalized per  $\Delta\Theta$  range). The black dots indicate sampling bins for which MOZAIC&CORE provide data from at least 20 flights.

the LMS close to the TTP ( $\Delta\Theta < 10$  K) are moister during the summer season. A key question here is to what extent this increase can be attributed to local transport from the underlying upper troposphere (UT) or to large-scale transport, particularly from monsoon-influenced regions. Further trajectory-based analysis is essential to quantify the contributions of the different transport mechanisms involved.

515

At levels of  $\Delta\Theta$  of around 20 K above the TTP, the highest values can be found during fall, with a maximum during October (Figure 11d), in contrast to a slight decrease from summer to fall in the LMS close to the TTP ( $\Delta\Theta < 10$  K) and in the UT ((Figure 11c,d). An increase of the exTL height during the fall season is a well-known feature for the northern extra-tropics,

as reported in various studies (e.g. Zahn et al., 2014). The reasons for the seasonal variability described in this section are not aimed to be discussed in detail in this paper (however, see e.g. Gettelman et al., 2011; Zahn et al., 2014) but will be the focus of future publications based on the adjusted MOZAIC&CORE climatologies.

~~Last but not least, we want to~~ Finally, we examine how well the climatology shown in Figure 11a-d cover the UT/LMS over the North Atlantic, given that passenger aircraft fly on constant altitudes and might avoid certain weather conditions. In order to investigate this, a sampling of  $\Delta\Theta$  and  $\Delta\varphi_{EQ}$  is applied to the ERA5 data. The probability density (normalized per  $\Delta\Theta$ ) based on ERA5 data from all vertical levels is shown in Figure 11. The dotted areas in the plots illustrate the sampling bins where IAGOS provides data from at least 20 flights. Overall, ~~a good coverage can be observed~~ good coverage is found. During winter and spring, only air masses in the UT below  $\Delta\Theta = -15$  K are not well covered (Figure 11a,b). During summer and fall (Figure 11d,e), air masses with an equivalent latitude of 30 - 40°N, i.e. of subtropical origin, are mostly not covered in the LMS which accounts to 20 - 30 % of all air masses. However, the most frequent air masses ( $\Delta\varphi_{EQ} = 50 - 80^\circ\text{N}$ ) are covered by IAGOS also during summer season.

## 5 Conclusion and Outlook

This study presented an algorithm to ~~adjust produce adjusted~~ H<sub>2</sub>O climatologies mean values in the lowermost stratosphere (LMS) ~~measured with based on measurements of~~ the compact IAGOS ~~humidity capacity capacitive humidity~~ sensor (ICH) operating onboard MOZAIC&CORE to the sophisticated measurements from IAGOS-CARIBIC. First, a statistical comparison of MOZAIC&CORE with CARIBIC H<sub>2</sub>O was conducted, selecting CARIBIC as the reference dataset due to its advanced instrumentation and similar spatial and temporal distribution. Although CARIBIC has a limited number of about 500 flights compared to around 60.000 flights by MOZAIC&CORE combined, it still provided a sufficient number of measurements for a valid intercomparison in the extratropical northern hemisphere.

For the comparison, a mapping approach was utilized, ~~applying a sampling of measurements where measurements were~~ sampled into bins of similar ~~origin, considering dynamical origin and properties. Consideration of~~ equivalent latitude, season, and height relative to the tropopause, were used to derive corresponding mean  $\text{RH}_{liq}$  values ( ~~$\overline{\text{RH}}_{liq}$  values~~  $\overline{\text{RH}}_{liq}$ ). Initially, CARIBIC data were compared with high-precision campaign measurements summarized in the JULIA data base. It was demonstrated that ~~CARIBIC measurements can detect~~ the CARIBIC H<sub>2</sub>O instrument package can quantify low stratospheric H<sub>2</sub>O concentrations of 10 ppmv or less, making them suitable for intercomparison with MOZAIC&CORE. However, it has to be regarded that JULIA ~~measurements were typically conducted under~~ and IAGOS measurements were, on average, conducted during different atmospheric conditions. While campaign flights often tend to take place during specific atmospheric conditions, ~~unlike the more statistically representative sampling by IAGOS flights passenger aircraft flights tend to avoid convective systems and other conditions with turbulent character (e.g. frontal systems)~~. Consequently, JULIA data were excluded from the comparison and adjustment of MOZAIC&CORE, as including them might introduce greater uncertainties rather than providing additional benefits from having more data.

The comparison between MOZAIC&CORE with CARIBIC showed good ~~agreements~~ agreement in the (extratropical) upper

troposphere. However, above the tropopause, the average values were generally biased, with the ~~discrepancy magnitude of the bias~~ increasing with distance ~~to the tropopause and reaching up to above the tropopause, reaching relative differences of 300 % relative differences for H<sub>2</sub>O~~ at around 5 ppmv. This systematic bias in the lower stratosphere was attributed to  
555 limitations of the ICH sensor, which loses sensitivity below approximately 10 % RH<sub>liq</sub>. Despite this, the sensors consistently performed well for mean values above 30 ppmv.

Subsequently, using the mapping approach, a method was developed to adjust  $\overline{\text{RH}}_{\text{liq}}$  from MOZAIC&CORE to those from CARIBIC. The biases were quantified as a function of  $\overline{\text{RH}}_{\text{liq}}$ , enabling the adjustment of MOZAIC&CORE H<sub>2</sub>O climatologies with an uncertainty of approximately 1 ppmv (winter) to 2.5 ppmv (summer) for mean values of 10 ppmv and less.

560 A caveat is that the adjustment of  $\overline{\text{RH}}_{\text{liq}}$  is based on a statistical comparison of the small CARIBIC reference dataset with the much larger MOZAIC&CORE dataset. This introduces a small systematic error due to the limited representativeness of the CARIBIC dataset. This representativeness error could be neglected for studies of variability and transport processes, but for H<sub>2</sub>O trend analyses this error must be considered and quantified. Nevertheless, due to the lack of in-situ measurements in the UT/LMS, the adjusted climatologies provide better resolution of temporal and spatial variability of UT/LMS H<sub>2</sub>O compared  
565 to other in-situ or space-borne datasets. This will contribute to a better understanding of the H<sub>2</sub>O variability in the extratropical UT/LMS and its connection to various transport and mixing processes. Based on the adjusted H<sub>2</sub>O climatologies, upcoming studies will investigate the contribution of different transport mechanisms to the H<sub>2</sub>O variability, using backward trajectories and simulations of (de-)hydration of air masses along their pathways. This enhanced understanding of the H<sub>2</sub>O variability and its corresponding transport mechanisms is crucial for improving the quality of model simulations concerning current and future  
570 H<sub>2</sub>O concentrations in the UT/LMS and their impact on the radiative forcing in a warming climate.

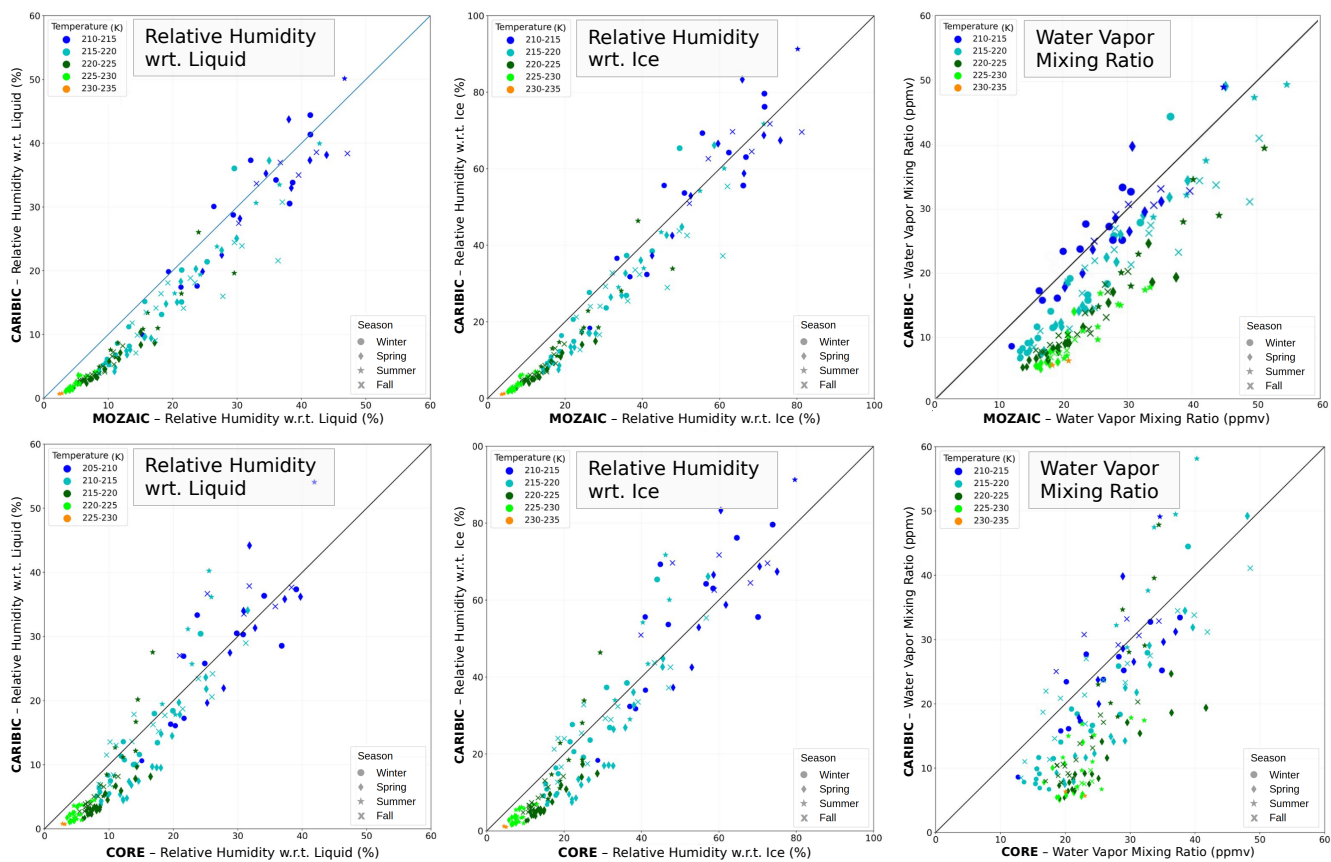


**Figure A1.** Intercomparison of sampled mean values of  $RH_{liq}$ ,  $RH_{ice}$  and  $H_2O$  for IAGOS-MOZAIC (top) and CORE (bottom) with IAGOS-CARIBIC. Instead of the height relative to the tropopause as shown in Figure 5, the colors indicate temperature ranges.

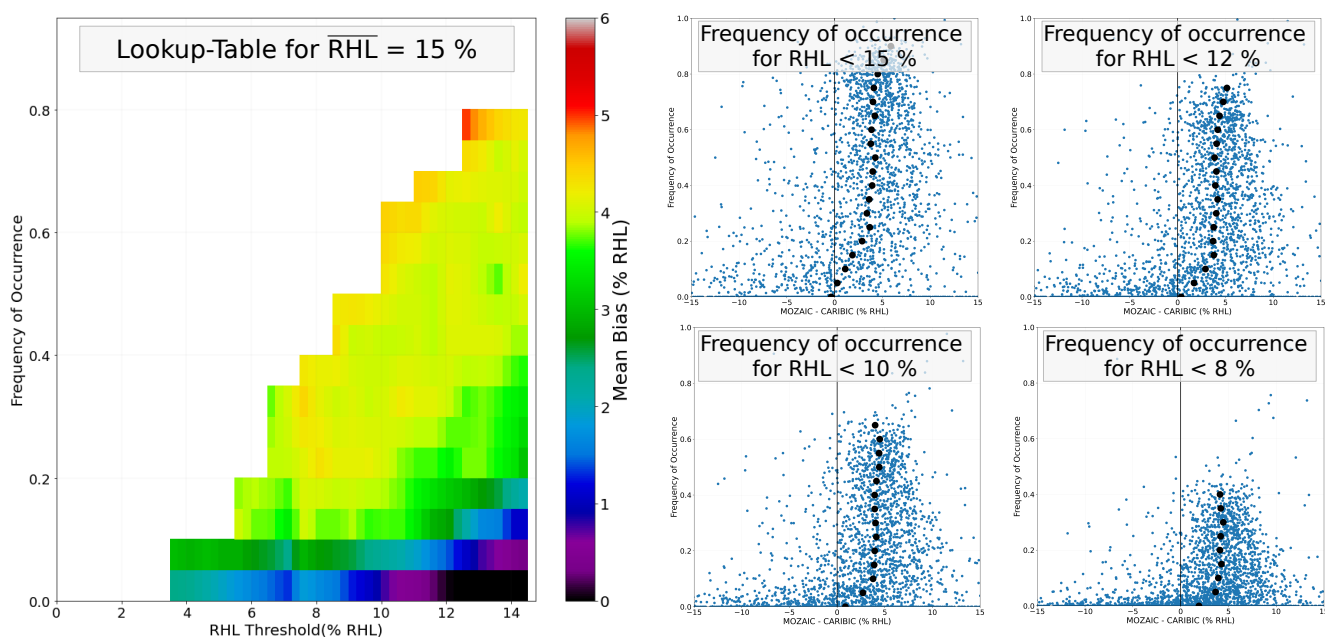


**Figure A2.** (a) Lookup-table for a mean value  $\overline{RH}_L$  of 15 % which will be used to adjust potentially biased mean values of 15 %. (b) Corresponding frequency of occurrence for exemplary thresholds that are the basis for the final lookup-table

. PK developed the methodology, performed the analysis, and wrote the manuscript. CR, MK, HB and AZ contributed to the development of the mapping and adjustment approach. HB and AZ provided and helped with analysing the IAGOS-CARIBIC dataset. AP, SR and YL provided and helped with analysing the IAGOS-CORE dataset

. At least one of the (co-)authors is a member of the editorial board of Atmospheric Chemistry and Physics. The authors have no other competing interests to declare.

. The study was funded by the Deutsche Forschungsgemeinschaft (DFG, German Research Foundation) – TRR 301 – Project-ID 428312742. Parts of the study were also funded by ESA (contract no. 4000123554) via the Water Vapour Climate Change Initiative (WV\_cci) project phase 2 of ESA’s Climate Change Initiative (CCI). We acknowledge the European Centre for Medium-Range Weather Forecasts (ECMWF) for their ERA-5 meteorological data. MOZAIC/CARIBIC/IAGOS data were created with support from the European Commission, national agencies in Germany (BMBF), France (MESR), and the UK (NERC), and the IAGOS member institutions (<http://www.iagos.org/partners>). The participating airlines (Lufthansa, Air France, Austrian, China Airlines, Hawaiian Airlines, Air Canada, Iberia, Eurowings Discover, Cathay Pacific, Air Namibia, Sabena) supported IAGOS by carrying the measurement equipment free of charge since 1994. The data are available at <http://www.iagos.fr> thanks to additional support from AERIS.

## References

- 585 Banerjee, A., Chiodo, G., Previdi, M., Ponater, M., Conley, A., and Polvani, L.: Stratospheric water vapor: an important climate feedback, *Climate Dynamics*, <https://doi.org/10.1007/s00382-019-04721-4>, 2019.
- Benjamin, S. G., Schwartz, B. E., and Cole, R. E.: Accuracy of ACARS Wind and Temperature Observations Determined by Collocation, *Weather and Forecasting*, 14, 1032 – 1038, [https://doi.org/10.1175/1520-0434\(1999\)014<1032:AOAWAT>2.0.CO;2](https://doi.org/10.1175/1520-0434(1999)014<1032:AOAWAT>2.0.CO;2), 1999.
- Berger, V. W. and Zhou, Y.: Kolmogorov–Smirnov Test: Overview, <https://doi.org/https://doi.org/10.1002/9781118445112.stat06558>, 2014.
- 590 Bethan, S., Vaughan, G., and Reid, S. J.: A comparison of ozone and thermal tropopause heights and the impact of tropopause definition on quantifying the ozone content of the troposphere, *Quarterly Journal of the Royal Meteorological Society*, 122, 929–944, <https://api.semanticscholar.org/CorpusID:121184239>, 1996.
- Dyroff, C., Zahn, A., Christner, E., Forbes, R., Tompkins, A. M., and van Velthoven, P. F. J.: Comparison of ECMWF analysis and forecast humidity data with CARIBIC upper troposphere and lower stratosphere observations, *Quarterly Journal of the Royal Meteorological*
- 595 *Society*, 141, 833–844, <https://doi.org/10.1002/qj.2400>, 2015.
- Engel, A., Bönisch, H., Brunner, D., Fischer, H., Franke, H., Günther, G., Gurk, C., Hegglin, M., Hoor, P., Königstedt, R., Krebsbach, M., Maser, R., Parchatka, U., Peter, T., Schell, D., Schiller, C., Schmidt, U., Spelten, N., Szabo, T., Weers, U., Wernli, H., Wetter, T., and Wirth, V.: Highly resolved observations of trace gases in the lowermost stratosphere and upper troposphere from the Spurt project: an overview, *Atmospheric Chemistry and Physics*, 6, 283–301, <https://doi.org/10.5194/acp-6-283-2006>, 2006.
- 600 Forster, P. M. d. F. and Shine, K. P.: Assessing the climate impact of trends in stratospheric water vapor, *Geophysical Research Letters*, 29, 10–1–10–4, <https://doi.org/10.1029/2001GL013909>, 2002.
- Gottelman, A., Hoor, P., Pan, L. L., Randel, W. J., Hegglin, M. I., and Birner, T.: THE EXTRATROPICAL UPPER TROPOSPHERE AND LOWER STRATOSPHERE, *Reviews of Geophysics*, 49, <https://doi.org/10.1029/2011RG000355>, 2011.
- Hegglin, M., Plummer, D., Shepherd, T., Scinocca, J., Anderson, J., Froidevaux, L., Funke, B., Hurst, D., Rozanov, A., Urban, J., Clarmann, T., Walker, K., Wang, H., Tegtmeier, S., and Weigel, K.: Vertical structure of stratospheric water vapour trends derived from merged
- 605 satellite data, *Nature Geoscience*, 7, 768–776, <https://doi.org/10.1038/ngeo2236>, 2014.
- Hegglin, M. I., Boone, C. D., Manney, G. L., Shepherd, T. G., Walker, K. A., Bernath, P. F., Daffer, W. H., Hoor, P., and Schiller, C.: Validation of ACE-FTS satellite data in the upper troposphere/lower stratosphere (UTLS) using non-coincident measurements, *Atmospheric Chemistry and Physics*, 8, 1483–1499, <https://doi.org/10.5194/acp-8-1483-2008>, 2008.
- 610 Hegglin, M. I., Tegtmeier, S., Anderson, J., Froidevaux, L., Fuller, R., Funke, B., Jones, A., Lingenfelter, G., Lumpe, J., Pendlebury, D., Remsberg, E., Rozanov, A., Toohey, M., Urban, J., von Clarmann, T., Walker, K. A., Wang, R., and Weigel, K.: SPARC Data Initiative: Comparison of water vapor climatologies from international satellite limb sounders, *Journal of Geophysical Research: Atmospheres*, 118, 11,824–11,846, <https://doi.org/https://doi.org/10.1002/jgrd.50752>, 2013.
- Hersbach, H., Bell, B., Berrisford, P., Hirahara, S., Horányi, A., Muñoz-Sabater, J., Nicolas, J., Peubey, C., Radu, R., Schepers, D., Simmons, A., Soci, C., Abdalla, S., Abellan, X., Balsamo, G., Bechtold, P., Biavati, G., Bidlot, J., Bonavita, M., De Chiara, G., Dahlgren, P., Dee, D., Diamantakis, M., Dragani, R., Flemming, J., Forbes, R., Fuentes, M., Geer, A., Haimberger, L., Healy, S., Hogan, R. J., Hólm, E., Janisková, M., Keeley, S., Laloyaux, P., Lopez, P., Lupu, C., Radnoti, G., de Rosnay, P., Rozum, I., Vamborg, F., Villaume, S., and Thépaut, J.-N.: The ERA5 global reanalysis, *Quarterly Journal of the Royal Meteorological Society*, 146, 1999–2049, <https://doi.org/10.1002/qj.3803>, 2020.

- 620 Huang, Y., Wang, Y., and Huang, H.: Stratospheric Water Vapor Feedback Disclosed by a Locking Experiment, *Geophysical Research Letters*, 47, <https://doi.org/10.1029/2020GL087987>, 2020.
- IPCC: Climate Change 2021 – The Physical Science Basis: Working Group I Contribution to the Sixth Assessment Report of the Intergovernmental Panel on Climate Change, <https://doi.org/10.1017/9781009157896>, 2023.
- Kirk-Davidoff, D., Hintsala, E., Anderson, J., and Keith, D.: The Effect of Climate Change on Ozone Depletion through Changes in  
625 Stratospheric Water Vapour, *Nature*, 402, <https://doi.org/10.1038/46521>, 1999.
- Konopka, P., Tao, M., Ploeger, F., Hurst, D. F., Santee, M. L., Wright, J. S., and Riese, M.: Stratospheric Moistening After 2000, *Geophysical Research Letters*, 49, e2021GL097609, <https://doi.org/https://doi.org/10.1029/2021GL097609>, e2021GL097609 2021GL097609, 2022.
- Krämer, M., Rolf, C., Spelten, N., Afchine, A., Fahey, D., Jensen, E., Khaykin, S., Kuhn, T., Lawson, P., Lykov, A., Pan, L. L., Riese, M., Rollins, A., Stroh, F., Thornberry, T., Wolf, V.,  
630 Woods, S., Spichtinger, P., Quaas, J., and Sourdeval, O.: A microphysics guide to cirrus – Part 2: Climatologies of clouds and humidity from observations, *Atmospheric Chemistry and Physics*, 20, 12 569–12 608, <https://doi.org/10.5194/acp-20-12569-2020>, 2020.
- Kunkel, D., Hoor, P., Kaluza, T., Ungermann, J., Kluschat, B., Giez, A., Lachnitt, H.-C., Kaufmann, M., and Riese, M.: Evidence of small-scale quasi-isentropic mixing in ridges of extratropical baroclinic waves, *Atmospheric Chemistry and Physics*, 19, 12 607–12 630,  
635 <https://doi.org/10.5194/acp-19-12607-2019>, 2019.
- Kunz, A., Schiller, C., Rohrer, F., Smit, H. G. J., Nedelec, P., and Spelten, N.: Statistical analysis of water vapour and ozone in the UT/LS observed during SPURT and MOZAIC, *Atmospheric Chemistry and Physics*, 8, 6603–6615, <https://doi.org/10.5194/acp-8-6603-2008>, 2008.
- Marenco, A., Thouret, V., Nedelec, P., Smit, H., Helten, M., D., K., Karcher, F., Simon, P., Law, K., Pyle, J. and Poschmann, G., von Wrede,  
640 R., Hume, C., and Cook, T.: Measurement of ozone and water vapor by Airbus in-service aircraft: The MOZAIC airborne program, an overview, *Journal of Geophysical Research: Atmospheres*, 103, 25 631–25 642, <https://doi.org/10.1029/98JD00977>, 1998.
- Meyer, J., Rolf, C., Schiller, C., Rohs, S., Spelten, N., Afchine, A., Zöger, M., Sitnikov, N., Thornberry, T. D., Rollins, A. W., Bozóki, Z., Tátraí, D., Ebert, V., Kühnreich, B., Mackrodt, P., Möhler, O., Saathoff, H., Rosenlof, K. H., and Krämer, M.: Two decades of water vapor measurements with the FISH fluorescence hygrometer: a review, *Atmospheric Chemistry and Physics*, 15, 8521–8538,  
645 <https://doi.org/10.5194/acp-15-8521-2015>, 2015.
- Millan, L. F., Manney, G. L., Boenisch, H., Hegglin, M. I., Hoor, P., Kunkel, D., Leblanc, T., Petropavlovskikh, I., Walker, K., Wargan, K., and Zahn, A.: Multi-parameter dynamical diagnostics for upper tropospheric and lower stratospheric studies, *Atmospheric Measurement Techniques*, 16, 2957–2988, <https://doi.org/10.5194/amt-16-2957-2023>, 2023.
- Neis, P., Smit, H., Rohs, S., Bundke, U., Krämer, M., Spelten, N., Ebert, V., Buchholz, B., Thomas, K., and Petzold, A.: Quality assessment of  
650 MOZAIC and IAGOS capacitive hygrometers: Insights from airborne field studies, *Tellus B*, 67, <https://doi.org/10.3402/tellusb.v67.28320>, 2015a.
- Neis, P., Smit, H. G. J., Krämer, M., Spelten, N., and Petzold, A.: Evaluation of the MOZAIC Capacitive Hygrometer during the airborne field study CIRrus-III, *Atmospheric Measurement Techniques*, 8, 1233–1243, <https://doi.org/10.5194/amt-8-1233-2015>, 2015b.
- Nowack, P., Ceppi, P., Davis, S. M., Chiodo, G., Ball, W., Diallo, M. A., Hassler, B., Jia, Y., Keeble, J., and Joshi, M.: Response of  
655 stratospheric water vapour to warming constrained by satellite observations, *Nat. Geosci.*, <https://doi.org/10.1038/s41561-023-01183-6>, 2023.

- Nützel, M., Podglajen, A., Garny, H., and Ploeger, F.: Quantification of water vapour transport from the Asian monsoon to the stratosphere, *Atmospheric Chemistry and Physics*, 19, 8947–8966, <https://doi.org/10.5194/acp-19-8947-2019>, 2019.
- 660 Petzold, A., Thouret, V., Gerbig, C., Zahn, A., Brenninkmeijer, C., Gallagher, M., Hermann, M., Pontaud, M., Ziereis, H., Boulanger, D., Marshall, J., Nédélec, P., Smit, H., Frieß, U., Flaud, J.-M., Wahner, A., Cammas, J.-P., and Volz-Thomas, A.: Global-scale atmosphere monitoring by in-service aircraft - current achievements and future prospects of the European Research Infrastructure IAGOS, *Tellus B*, 67, <https://doi.org/10.3402/tellusb.v67.28452>, 2015.
- Petzold, A., Neis, P., Rütimann, M., Rohs, S., Berkes, F., Smit, H. G. J., Krämer, M., Spelten, N., Spichtinger, P., Nédélec, P., and Wahner, A.: Ice-supersaturated air masses in the northern mid-latitudes from regular in situ observations by passenger aircraft: vertical distribution, 665 seasonality and tropospheric fingerprint, *Atmospheric Chemistry and Physics*, 20, 8157–8179, <https://doi.org/10.5194/acp-20-8157-2020>, 2020.
- Riese, M., Ploeger, F., Rap, A., Vogel, B., Konopka, P., Dameris, M., and Forster, P.: Impact of uncertainties in atmospheric mixing on simulated UTLS composition and related radiative effects, *J. Geophys. Res.*, 117, D16 305, <https://doi.org/10.1029/2012JD017751>, 2012.
- Rolf, C., Rohs, S., Smit, H., Krämer, M., Bozóki, Z., Hofmann, S., Franke, H., Maser, R., Hoor, P., and Petzold, A.: Evaluation of compact 670 hygrometers for continuous airborne measurements, *Meteorologische Zeitschrift*, pp. –, <https://doi.org/10.1127/metz/2023/1187>, 2023.
- Smit, H. G. J., Volz-Thomas, A., Helten, M., Paetz, W., and Kley, D.: An In-Flight Calibration Method for Near-Real-Time Humidity Measurements with the Airborne MOZAIC Sensor, *Journal of Atmospheric and Oceanic Technology*, 25, 656 – 666, <https://doi.org/10.1175/2007JTECHA975.1>, 2008.
- Sprung, D. and Zahn, A.: Acetone in the upper troposphere/lowermost stratosphere measured by the CARIBIC 675 passenger aircraft: Distribution, seasonal cycle, and variability, *Journal of Geophysical Research: Atmospheres*, 115, <https://doi.org/https://doi.org/10.1029/2009JD012099>, 2010.
- Tang, W., Howell, G., and Tsai, Y.-H.: Barometric altimeter short-term accuracy analysis, *IEEE Aerospace and Electronic Systems Magazine*, 20, 24–26, <https://doi.org/10.1109/MAES.2005.1576100>, 2005.
- Tatrai, D., Bozóki, Z., Smit, H., Rolf, C., Kraemer, M., Filges, A., Gerbig, C., Gulyás, G., and Szabo, G.: Dual channel photoacoustic 680 hygrometer for airborn measurements: Background, calibration, laboratory and in-flight inter-comparison tests, *Atmospheric Measurement Techniques*, 8, 33–42, <https://doi.org/10.5194/amt-8-33-2015>, 2015.
- Zahn, A., Christner, E., Velthoven, P., Rauthe-Schöch, A., and Brenninkmeijer, C.: Processes controlling water vapor in the upper troposphere/lowermost stratosphere: An analysis of 8 years of monthly measurements by the IAGOS-CARIBIC observatory: CARIBIC H<sub>2</sub>O in the UT/LMS, *Journal of Geophysical Research: Atmospheres*, 119, <https://doi.org/10.1002/2014JD021687>, 2014.
- 685 Zöger, M., Afchine, A., Eicke, N., Gerhards, M.-T., Klein, E., McKenna, D. S., Mörschel, U., Schmidt, U., Tan, V., Tuitjer, F., Woyke, T., and Schiller, C.: Fast in situ stratospheric hygrometers: A new family of balloon-borne and airborne Lyman  $\alpha$  photofragment fluorescence hygrometers, *Journal of Geophysical Research: Atmospheres*, 104, 1807–1816, <https://doi.org/10.1029/1998JD100025>, 1999.